Running Head: PRX01, PRX44 and PRX73 are peroxidases active in root hair growth

Authors for Correspondence:

José M. Estevez

Fundación Instituto Leloir, Av. Patricias Argentinas 435, Buenos Aires C1405BWE, Argentina. TE: 54-115238-7500 EXT. 3206

Centro de Biotecnología Vegetal, Facultad de Ciencias de la Vida, Universidad Andrés Bello and Millennium Institute for Integrative Biology (iBio), Santiago CP 8370146, Chile.

Email: jestevez@leloir.org.ar / jose.estevez@unab.cl

Research area most appropriate for paper: Plant Biology

Text Word count: 3,667

Figures 1-4

Table 1

Experimental procedures

References: 55

RESEARCH REPORT

Class III peroxidases PRX01, PRX44, and PRX73 potentially target extensins during root hair growth in *Arabidopsis thaliana*

Eliana Marzol[1,#], Cecilia Borassi[1,#], Philippe Ranocha[2], Ariel. A. Aptekman[3,4], Mauro Bringas[5], Janice Pennington[6], Julio Paez-Valencia[6], Javier Martínez Pacheco[1], Diana Rosa Rodríguez Garcia[1], Yossmayer del Carmen Rondón Guerrero[1], Mariana Carignani[1], Silvina Mangano[1], Margaret Fleming[7], John W. Mishler-Elmore[8], Francisca Blanco-Herrera[9,10], Patricia Bedinger[7], Christophe Dunand[2], Luciana Capece[5], Alejandro D. Nadra[3,4], Michael Held[8], Marisa Otegui[6,11] & José M. Estevez[1,9,†]

[1]Fundación Instituto Leloir and IIBBA-CONICET. Av. Patricias Argentinas 435, Buenos Aires C1405BWE, Argentina.
[2]Université de Toulouse, UPS, UMR 5546, Laboratoire de Recherche en Sciences Végétales, F-31326 CNRS, UMR 5546 Castanet-Tolosan, France.
[3]Departamento de Fisiología, Biología Molecular y Celular, Instituto de Biociencias, Biotecnología y Biología Traslacional (iB3). Facultad de Ciencias Exactas y Naturales, Universidad de Buenos Aires, Ciudad Universitaria, Buenos Aires C1428EGA, Argentina.
[4]Departamento de Química Biológica, Facultad de Ciencias Exactas y Naturales, Universidad de Buenos Aires (IQUIBICEN-CONICET), Ciudad Universitaria, Buenos Aires C1428EGA, Argentina.
[5]Departamento de Química Inorgánica, Analítica y Química Física, Facultad de Ciencias Exactas y Naturales, Universidad de Buenos Aires (INQUIMAE-CONICET), Buenos Aires, CP. C1428EGA, Argentina.
[6]Laboratory of Cell and Molecular Biology, University of Wisconsin, Madison, WI, USA.
[7]Department of Biology, Colorado State University, Fort Collins, Colorado 80523-1878, USA.
[8]Department of Chemistry and Biochemistry, Ohio University, Athens, OH 45701, USA.
[9]Centro de Biotecnología Vegetal, Facultad de Ciencias de la Vida, Universidad Andrés Bello and Millennium Institute for Integrative Biology (iBio), Santiago, Chile.
[10]Center of Applied Ecology and Sustainability (CAPES), Chile.
[11]Departments of Botany and Genetics, University of Wisconsin, Madison, WI, USA.

[#]co-first authors
[†] Correspondence should be addressed. Email: jestevez@leloir.org.ar / jose.estevez@unab.cl (J.M.E).

Key words: Arabidopsis, cell walls, extensins, root hairs, ROS, class-III peroxidases.

Word count: 3,656

Abstract

- Root hair cells are important sensors of soil conditions. Expanding several hundred times their original size, root hairs grow towards and absorb water-soluble nutrients. This rapid growth is oscillatory and is mediated by continuous remodelling of the cell wall. Root hair cell walls contain polysaccharides and hydroxyproline-rich glycoproteins including extensins (EXTs).

- Class-III peroxidases (PRXs) are secreted into the apoplastic space and are thought to trigger either cell wall loosening, mediated by oxygen radical species, or polymerization of cell wall components, including the Tyr-mediated assembly of EXT networks (EXT-PRXs). The precise role of these EXT-PRXs is unknown.

- Using genetic, biochemical, and modeling approaches, we identified and characterized three root hair-specific putative EXT-PRXs, PRX01, PRX44, and PRX73. The triple mutant *prx01,44,73* and the PRX44 and PRX73 overexpressors had opposite phenotypes with respect to root hair growth, peroxidase activity and ROS production with a clear impact on cell wall thickness.

- Modeling and docking calculations suggested that these three putative EXT-PRXs may interact with non-*O*-glycosylated sections of EXT peptides that reduce the Tyr-to-Tyr intra-chain distances in EXT aggregates and thereby may enhance Tyr crosslinking. These results suggest that these three putative EXT-PRXs control cell wall properties during the polar expansion of root hair cells.

Word count: 200

Introduction

Primary cell walls composed by a diverse network of polysaccharides and structural glycoproteins, regulate cell elongation, which is crucial for several plant growth and developmental processes. Extensins (EXTs) belong to hydroxyproline (Hyp)-rich glycoprotein (HRGP) superfamily and broadly include related glycoproteins such as proline-rich proteins (PRPs) and leucine-rich repeat extensins (LRXs) with multiple Ser-$(Pro)_{3–5}$ repeats that may be *O*-glycosylated and contain Tyr (Y)-based motifs (Marzol et al. 2018). EXTs require several modifications before they become functional (Marzol et al. 2018). After being hydroxylated and *O*-glycosylated in the secretory pathway, the secreted *O*-glycosylated EXTs are crosslinked and insolubilized in the plant cell wall by the activity of secreted class-III peroxidases (PRXs) on the Tyr-based motifs (Lamport et al., 2011; Marzol et al. 2018). PRXs are thought to facilitate both intra and inter-molecular covalent Tyr–Tyr crosslinks in EXT networks, possibly through the assembly of triple helices (Velasquez et al. 2015) by generating *iso*dityrosine units (IDT) and pulcherosine, or di-*iso*dityrosine (Di-IDT), respectively (Brady et al., 1996; 1998; Held et al. 2004). However, the underlying molecular mechanisms of EXT crosslinking and assembly have not been determined. The presence of Tyr-mediated crosslinking in EXT and related glycoproteins allow them to form a dendritic glycoprotein network in the cell wall. This network affects *de novo* cell wall formation during embryo development (Cannon *et al.*, 2008) and in polar cell expansion processes in root hairs (Baumberger 2001, 2003; Ringli 2010; Velasquez et al. 2011; 2012; 2015a,b) and pollen tubes (Ringli et al. 2017; Sede et al. 2018; Wang et al. 2018).

Apoplastic class-III PRXs are heme-iron-dependent proteins, members of a large multigenic family in land plants, with 73 members in *Arabidopsis thaliana* (Passardi et al. 2004; Weng and Chapple, 2010). These PRXs catalyze several different classes of reactions. PRX activities coupled to $_{apo}$ROS molecules ($_{apo}H_2O_2$) directly affect the degree of cell wall crosslinking (Dunand et al. 2007) by oxidizing cell wall compounds and leading to stiffening of the cell wall through a peroxidative cycle (PC) (Lamport et al. 2011). By constrast, $_{apo}$ROS coupled to PRX activity enhances non-enzymatic cell wall-loosening by producing oxygen radical species (e.g., $^{\cdot}OH$) and promoting growth in the hydroxylic cycle (HC). It is unclear how these opposite effects on cell wall polymers are coordinated during plant growth (Passardi et al. 2004, Cosio & Dunand 2009). Finally, PRXs also contribute to the superoxide radical ($O_2^{\cdot-}$) pool by oxidizing singlet oxygen in the oxidative cycle (OC), thereby affecting $_{apo}H_2O_2$ levels. Thus, several PRXs are involved in the oxidative polymerization of monolignols in the apoplast of the lignifying cells in xylem (e.g. PRX017; Cosio et al 2017), in the root endodermis (e.g. PRX64; Lee et al. 2013; Ropollo et al. 2011), and in petal detachment (Lee et al 2018). In addition, PRXs are able to polymerize other components of the plant cell wall such as suberin, pectins, and EXTs (Schnabelrauch *et al.*, 1996; Bernards et al., 1999; Jackson et al., 2001; Francoz et al. 2019). Although several candidates of PRXs have been associated specifically with EXT-crosslinking (EXT-PRXs) by *in vitro* studies (Schnabelrauch et al., 1996; Wojtaszek et al., 1997; Jackson et al., 2001; Price et al., 2003; Pereira et al. 2011; Dong et al., 2015) or immunolabelling

extension characterization (Jacobowitz et al. 2019), the *in vivo* characterization and mode of action of these EXT-PRXs remain largely unknown. In this work, we used a combination of reverse genetics, molecular and cell biology, computational molecular modeling, and biochemistry to identify three apoplastic PRXs, PRX01, PRX44 and PRX73, as key enzymes possibly involved in Tyr-crosslinking of cell wall EXTs in growing root hair cells. In addition, we propose a model in which *O*-glycosylation levels on the triple helixes of EXTs regulate the degree of Tyr-crosslinking affecting the expansion properties of cell walls as suggested before (Velasquez et al. 2015a). Our results open the way for the discovery of similar interactions during root hair development and in response to the environmental changes, such fluctuating nutrient availability in the soil.

Results and Discussion

In this work, we have chosen to analyze root hair cells because they are an excellent model for tracking cell elongation and identifying PRXs involved in EXT assembly. In previous work, the phenotypes of mutants for PRX01, PRX44 and PRX73 suggested that these PRXs are involved in root hair growth and ROS homeostasis, although their mechanisms of action remained to be characterized (Mangano et al. 2017). All three PRXs are under the transcriptional regulation of the root hair specific transcription factor RSL4 (Yi et al. 2010; Mangano et al. 2017). As expected, these three PRXs are also highly co-expressed with other root hair-specific genes encoding cell wall EXTs (e.g., EXT6-7, EXT12-14, and EXT18) and EXT-related glycoproteins (e.g. LRX1 and LRX2), which functions in cell expansion (Ringli 2010; Velasquez et al. 2011; Velasquez et al. 2015b) (**Figure S1**). Based on this evidence, we hypothesized that these three PRXs might be EXT-PRXs and catalyze Tyr-crosslinks to assemble EXTs in root hair cell walls.

To confirm that PRX01, PRX44, and PRX73 are expressed specifically in root hairs, we made transcriptional reporters harboring GFP-tagged fusions of the promoter regions of their genes. In agreement with the *in silico* database (Mangano et al. 2017 and **Figure S1**), all three genes were strongly expressed in root hair cells during cell elongation (**Figure 1A**). Single and double mutants for these three PRXs showed almost normal root hair growth (Mangano et al. 2017), suggesting a high degree of functional redundancy. By contrast, a triple null mutant, *prx01,44,73*, showed much shorter root hair cells (**Figure 1B**) than what was previously reported for each of the individual *prx* mutants (Mangano et al. 2017). We also obtained two independent lines overexpressing each of the PRXs fused to GFP and under the control of a strong *35SCaMV* promoter (PRX^{OE}). Unlike the *prx01,44,73* mutant, the lines overexpressing PRX44 and PRX73 had significantly longer root hairs than the Wt Col-0 control (**Figure 2A–B**). The root hairs of the $PRX01^{OE}$ lines, however, were similar to those of Wt Col-0 (**Figure 2A–B**). We reasoned that the lack of enhanced root hair expansion in the $PRX01^{OE}$ lines could be due to reduced levels of overexpression compared to the $PRX44^{OE}$ and $PRX73^{OE}$ lines. However, based on the GFP signals in intact roots (**Figure 2C**) and immunoblot analysis of protein extracts with anti-GFP antibodies (**Figure 2D**), we established that PRX01-GFP and

PRX44-GFP are strongly expressed, whereas PRX73-GFP showed more moderate expression. Furthermore, the three PRX-GFP-fusion proteins were detected at the expected molecular weights in an immunoblot (**Figure 2D**), indicating that the tagged proteins are stable. Together, these results highlight the partially redundant but not identical roles of PRX01, PRX44, and PRX73 as positive regulators of polar growth. This is in agreement with the negative effect of SHAM, which blocks the activity of most peroxidases, on root hair growth (Mangano et al. 2017).

To confirm that our mutant and overexpressing lines had the expected changes in peroxidase activity, we measured *in vitro* total peroxidase activity using a guaiacol oxidation-based assay. The *prx01,44,73* roots showed reduced peroxidase activity (close to 50% reduction) (**Figure 1C**), whereas there was a 40–50% increase in PRX73^{OE} and an approximately 20% increase in PRX44^{OE} (**Figure 2E**). Consistent with our root hair growth analysis (**Figure 2A**), PRX01^{OE} showed normal peroxidase activity (**Figure 2E**). These three PRXs might consume ROS, most probably H_2O_2, for their catalytic functions in the cell wall/apoplast. Therefore, we measured cytoplasmic ROS ($_{cyt}$ROS) levels by oxidation of H_2DCF-DA and apoplastic ROS ($_{apo}$ROS) levels with the Amplex Ultra Red (AUR) probe in root hair tips. The *prx01,44,73* root hair tips showed lower levels of $_{cyt}$ROS (**Figure 1D**) but increased $_{apo}$ROS accumulation (**Figure 1E**) compared to Wt Col-0. The $_{apo}$ROS levels were similar in PRX01^{OE}, and slightly lower in PRX44^{OE}, and PRX73^{OE} lines when compared to Wt Col-0 (**Figure 2F**). These results suggest that PRX01, PRX44, and PRX73 function as apoplastic regulators of ROS-linked root hair cell elongation.

Next, to further analyze the ultrastructure of the cell wall in growing root hairs, we analyzed Wt Col, PRX44^{OE}, and *prx01,44,73* triple mutant roots treated with or without SHAM by transmission electron microscopy (**Figure 3A**). Much found thinner cell walls at the root hair tips of PRX44^{OE} (0.74 ±0.24 µm for PRX44^{OE}) and *prx01,44,73* (0.61 ±0.14 µm) when compared to Wt Col-0 plants (1.2 ±0.3 µm for Wt) (**Figure 3B**). SHAM treatment caused a statistically significant increase in cell wall thickness in the PRX44^{OE} and *prx01,44,73* root hairs (**Figure 3B**), but not in Wt Col-0. This result confirms the importance of peroxidase activity in cell wall structure and highlights that either depletion of PRX01,44,73 (triple mutant) or the overexpression of PRX44 results in an overall reduction in cell wall thickness in growing root hairs.

Then, we designed an EXT reporter to track EXT secretion and PRX-mediated insolubilization in the cell walls during root hair cell elongation. The secreted EXT reporter carries a Tomato tag (SS-TOM-Long-EXT) that is fluorescent under the acidic pH (Shen et al. 2014) that is typical of plant cell walls and apoplastic spaces (Stoddard & Rolland 2018). A secreted Tomato tag (ss-TOM) was used as a control (**Figure S2A**). The EXT domain includes only two Tyr, which are at the C-terminus and separated by 10 amino acids (Stratford et al., 2001). Expression of the EXT reporter was first tested in onion (*Allium cepa*) cells, and then the reporter was stably expressed in Arabidopsis root hairs

(**Figure S2C-F**). In both cases, plasmolysis was used to retract the plasma membrane from the cell surface to show that the EXT reporter was localized in the cell walls. Using immunoblot analysis, we detected the full-length EXT-Tomato fusion protein, with possible *O*-glycan modifications, running as higher molecular weight bands (**Figure S2B**). Importantly, the EXT reporter did not interfere with the polar growth of root hairs (**Figure S2D**), and, therefore, could be used to track changes in the *in situ* arrangement of cell wall EXTs. SS-TOM-Long-EXT is clearly insolubilized in the cell wall of growing root hairs (**Figure S2C**) but remains to be tested if these EXT reporter is mislocalized under an inhibited PRX environment (SHAM treated) or in *prx01,44,73* mutant background.

We then assessed the level of crosslinking of EXT Tyr residues by measuring peptidyl-tyrosine (Tyr) and isodityrosine (IDT, dimerized Tyr) in EXT extracted from whole roots. We detected a significant increase in peptidyl-Tyr in the *prx01,44,73* triple mutant relative to Wt Col-0, and slightly higher levels of IDT in EXTs extracted from the PRX73^{OE} line (**Table S1**). By contrast, we identified strong downregulation of Tyr- and IDT-levels in the EXT under-*O*-glycosylation mutants *p4h5*, *sergt1-1*, and *sergt1-1 rra3* (**Table 1**). PROLYL 4-HYDROXYLASE (P4H5), PEPTIDYL-SER GALACTOSYLTRANSFERASE (SERGT1), and REDUCE RESIDUAL ARABINOSE 3 (RRA3) are enzymes that modify EXT hydroxylation and *O*-glycosylation (**Table 1**). These results are consistent with the notion that *O*-glycans strongly affect EXT Tyr crosslinking, as was previously suggested based on the drastically reduced root hair growth of the under-glycosylation mutants and *in vitro* crosslinking rates (Velasquez et al 2015a,b; Chen et al. 2015). We hypothesize that absent or low *O*-glycosylation of EXTs or an increase in PRX levels may trigger a reduction in the amount of peptidyl-Tyr and IDT in EXTs, with a putative concomitant increase in the amounts of higher-order Tyr crosslinks (trimers and tetramers), thus inhibiting root hair growth. Further research is needed to decipher the *in vivo* regulation of Tyr crosslinking of EXTs by PRXs in plant cells.

A major limitation in our understanding of how EXTs function in plant cell walls is the lack of a realistic full-length EXT protein model. Previously, we generated preliminary versions of a short EXT triple-helix model (Velasquez et al. 2015a). To gain a more detailed understanding of how EXT molecules might operate in the plant cell wall, we used a coarse-grained molecular dynamics approach to build a larger model of a triple-helix EXT sequence that includes 10 conserved repeats (SPPPPYVYSSPPPPYYSPSPKVYYK) with a total length of 750 amino acids (250 in each polypeptide chain) (**Figure S3A–B**). Parameters for the *O*-glycosylated form of EXT were developed in this work, and we were able to simulate the EXT *O*-glycosylated system (**Figure S4**). The EXT molecules were modeled in two different states: as a non-glycosylated trimeric helical conformation similar to animal collagen, as performed previously (Velasquez et al., 2015a), and in the fully *O*-glycosylated state. In addition, we generated molecular dynamics simulations restraining both ends of the polypeptide chains, to model a fully extended helix (consistent with an “indefinitely long-EXT”). We also generated simulations without that restriction, to evaluate the conformation that an isolated

10-repeat triple helix would adopt. The results obtained in these simulations indicate the importance of the triple-helix conformation in the overall stability of the protein and especially in the conservation of its fibril-like structure, in agreement with 10-repeat single helix simulations performed previously (Marzol et al. 2018). The total volume of the extended 10-repeat triple helix was measured in both glycosylation states (**Table S1**), differentiating EXT-protein + *O*-glycans and EXT-protein-only volumes for the fully *O*-glycosylated EXT state. We observed that the EXT-protein-only volume was significantly augmented by the presence of the oligosaccharide moieties, indicating that *O*-glycans increase the distance between peptide chains in the EXT triple helix. We also report the average diameters for those systems (**Table S1**), which are consistent with the diameters previously reported based on atomic force microscopy images (Cannon et al. 2008). Additionally, *O*-glycosylation contributes to an increase in the average distance between the side chains of tyrosine residues, decreasing the proportion of tyrosine side chains that are close enough to lead to crosslinked EXT chains (**Figure S3C**). Current experimental and modeling lines of evidence are in agreement with the proposed role of proline-hydroxylation and carbohydrate moieties in keeping the EXT molecule in an extended helical polyproline-II conformation state (Stafstrom & Staehelin 1986; Owen et al., 2010; Ishiwata et al., 2014). This extended conformation might allow EXTs to interact properly with each other and with other components in the apoplast, including PRXs and pectins, to form a proper cell wall network (Nuñez et al., 2009; Valentin et al., 2010).

To test if the three PRXs (PRX01, PRX44, and PRX73) we identified might be able to interact directly with single-chain EXTs, we performed homology modeling with GvEP1 (from *Vitis vinifera*), an EXT-PRX that is able to crosslink EXTs *in vitro* (Jackson et al., 2001; Pereira et al. 2011). As additional controls, we selected PRX64, which has been described as necessary for lignin polymerization in Casparian strips in Arabidopsis root endodermis (Lee et al. 2013), and PRX36, which is able to bind homogalacturonan pectin in the outer seed coat layer (Francoz et al. 2019). By *docking* analysis, we obtained interaction energies (Kcal/mol) for PRX01, PRX44, PRX73, EXT-PRX GvEP1, and PRX64/PRX36. We analyzed docking with four different short EXT peptides: a non-hydroxylated EXT peptide $(SPPPYVY)_3$, a hydroxylated but not *O*-glycosylated EXT peptide $[(SOOOYVY)_3$; O=hydroxyproline], an EXT peptide that was only arabinosylated $[(SOOOYVY)_3$-A], and an arabino-galactosylated EXT peptide $[(SOOOYVY)_3$-AG]. As mentioned earlier, it was previously shown that mutants carrying under-*O*-glycosylated EXTs have severe defects in root hair growth (Velasquez et al. 2011; Velasquez et al. 2015a). At least one of these mutants, *p4h5*, also has a modified cell wall structure in the root hair tip (Velasquez et al. 2015b). Our docking results for the different PRXs show consistent interaction energy differences that depend on the glycosylation state of the EXT peptide used in the analysis, being higher for non-*O*-glycosylated species (both as proline or hydroxyproline). In addition, *O*-glycosylated EXT variants docked in a rather dispersed way while non-*O*-glycosylated variants preferentially docked in a grooved area (**Figure 4A–C**). Furthermore, **Figure 4A** shows how a non-*O*-glycosylated peptide binds through a groove, leaving one Tyr docked

in a cavity open to the solvent and very close to the heme iron (5Å), with a second Tyr a few Angstroms away. This disposition and the distances between the tyrosines suggest that this could be an active site where Tyr crosslinking takes place.

It is not possible to do a rigorous direct comparison of the interaction energies obtained with the different EXT species because of the different size and degree of freedom (depending on the *O*-glycosylation) among docking runs (**Figure 4B**). However, general trends can be observed in **Figure 4C**. In general, we observed higher interaction energies (more negative values) for hydroxylated species, followed by non-hydroxylated, and then by *O*-glycosylated variants. When we compared interaction energies among different PRXs interacting with EXT substrates with the same degree of *O*-glycosylation, we observed that PRX73 displayed the highest interaction activity with the non-hydroxylated (Ser-Pro-Pro-Pro) species, followed by PRX01 and then PRX44. For the hydroxylated, non-*O*-glycosylatied variant (Ser-Hyp-Hyp-Hyp), the order was PRX44>PRX73>PRX01. PRX44 displayed the highest interaction energy with the *O*-glycosylated species. All together, these results are consistent with the constitutive root hair growth effect observed for $PRX44^{OE}$ and $PRX73^{OE}$ and with non-glycosylated EXT being the substrate of peroxidation. Overall, this possibly indicate that PRX44 and PRX73 might interact with EXT substrates and possibly catalyze Tyr-crosslinking in open regions of the EXT backbones with little or no *O*-glycosylation. This is in agreement with previous studies that suggested that high levels of *O*-glycosylation in certain EXT segments physically restrict EXT lateral alignments, possibly by acting as a branching point (Velasquez et al., 2015a). Overall, the results of our study show that PRX01, PRX44, and PRX73 might be able good candidates for the crosslink EXTs at Tyr-sites.

To examine the evolution of PRX01, PRX44, and PRX73, we performed comprehensive phylogenetic analyses of Class-III peroxidases across diverse land plant lineages. Under low selective pressure to maintain substrate specificity, EXT-PRX activities might have evolved multiple times in parallel during land plant evolution through gene duplication followed by neofunctionalization or subfunctionalization. PRX01, PRX44, and PRX73 belong to three independent orthologous groups (**Figure S5**) and orthologs for each *A. thaliana* PRX have been detected in available Brassicaceae genomes and in various Angiosperm and Gymnosperm families, but not from Lycophytes and from non-vascular land plants. Thus, these three PRX sequences were the result of ancestral duplications before the divergence between Gymnosperms and Angiosperms but after the emergence of the Tracheophytes (**Figure S5**). Orthologs of the three PRX genes have only been detected in true root containing organisms and these three PRXs are expressed in roots and root hairs, as are most of their orthologous sequences (where expression data are available) (**Figure S6**). This strongly supports the hypothesis that the three independent orthogroups have conserved functions in roots. With the exception of PRX73, which belongs to a cluster containing the EXT-PRX from tomato (*Solanum lycopersicum*; LePRX38), the other two PRX sequences did not cluster with sequences

already described as putative EXT-PRXs, such as PRX09 and PRX40 (Jacobowitz et al. 2019). Indeed, the other known EXT-PRXs (identified mostly based on *in vitro* evidence) are not clustered together, but are widely distributed in the tree (**Figure S5**). This analysis suggests that plant EXT-PRXs might have evolved several times in parallel during Tracheophyte evolution.

Based on the results shown in this work, we propose a working model in which PRX01, PRX44, and PRX73 (and possibly other PRXs) control root hair growth by channelling H_2O_2 consumption and affecting the cell wall hardening process. In addition, high levels of ROS in the apical zone of the cytoplasm might activate many other processes also related to polar growth (**Figure S7**). By contrast, when apoplastic PRX protein levels are low, which is linked to reduced peroxidase activity (as in the triple mutant *prx01,44,73*), high levels of ROS (as H_2O_2) might accumulate in the apoplast, triggering through the oxidative cycle a cell wall loosening effect that affects growth homeostasis and inhibits expansion (**Figure S7**). Concomitantly, deficient PRX activity in the apoplast also triggers lower ROS levels in the cytoplasm of growing root hairs, decreasing root hair growth and cell wall thickness. Our results suggest that either lower or higher levels of apoplastic Class III PRXs in the root hair cell walls might affect the homeostasis of ROS and cell wall thickness with a clear effect on cell expansion. Still several aspects of this model proposed here remains to be tested.

Conclusions

Currently, several of the 73 apoplastic Class-III PRXs in *Arabidopsis thaliana* have no assigned biological function. In this work, we have characterized three related EXT-PRXs, PRX01, PRX44, and PRX73 that function in ROS homeostasis and possibly in EXT assembly during root hair growth. These PRXs might control Tyr crosslinking in EXTs and related glycoproteins and modify its secretion and assembly in the nascent tip cell walls. Using modeling and docking approaches, we were able to measure the interactions of these PRXs with single chain EXT substrates. All these lines of evidence indicate that PRX01, PRX44, and PRX73 are important enzymes that could be involved in EXT assembly during root hair growth. From an evolutionary perspective, all the putative EXT-PRXs (identified mostly based on *in vitro* evidence or immunolabeling) do not cluster together in the phylogenetic tree of Class-III PRXs, suggesting that plant-related EXT-PRXs might have evolved several times in parallel during Traqueophyte evolution. Interestingly, as a convergent evolutionary extracellular assembly, hydroxyproline-rich collagen Class-IV, similar to the green EXT linage and related glycoproteins, is also crosslinked by the activity of a specific class of animal heme peroxidases (named peroxidasin or PXDN) to form insoluble extracellular networks (Vanacore et al. 2009; Bhave et al. 2012). While the biophysical properties of collagen IV allow the correct development and function of multicellular tissues in all animal phyla (Brown et al. 2017), EXT assemblies also have key functions in several plant cell expansion and morphogenesis processes (Cannon *et al.*, 2008; Velasquez et al. 2015b; Marzol et al. 2018). This might imply that crosslinked extracellular matrices based on hydroxyproline-rich polymers (e.g., collagens and EXTs) have

345 evolved more than once during eukaryotic evolution, providing mechanical support to single and
346 multiple cellular tissues. Further analyses are required to establish how these EXT-PRXs catalyze Tyr
347 crosslinks on EXTs at the molecular level and how this assembly process is regulated during polar
348 cell expansion.

Experimental Procedures

Plant and growth conditions. *Arabidopsis thaliana* Columbia-0 (Col-0) was used as the wild Class (Wt) genotype in all experiments. All mutants and transgenic lines tested are in this genetic background. Seedlings were germinated on agar plates in a Percival incubator at 22°C in a growth room with 16h light/8h dark cycles for 10 days at 140 µmol $m^{-2}s^{-1}$ light intensity. Plants were transferred to soil for growth under the same conditions. For identification of T-DNA knockout lines, genomic DNA was extracted from rosette leaves. Confirmation by PCR of a single and multiple T-DNA insertions in the target PRX genes were performed using an insertion-specific LBb1 or LBb1.3 (for SALK lines) primer in addition to one gene-specific primer. To ensure gene disruptions, PCR was also run using two gene-specific primers, expecting bands corresponding to fragments larger than in WT. We isolated homozygous lines for PRX01 (AT1G05240, *prx01-2*, Salk_103597), PRX44 (AT4G26010, *prx44-2*, Salk_057222) and PRX73 (AT5G67400, *prx73-3*, Salk_009296).

PRX::GFP and 35S::PRX-GFP lines. Vectors based on the Gateway cloning technology (Invitrogen) were used for all manipulations. Constitutive expression of PRXs-GFP tagged lines were achieved in plant destination vector pMDC83. cDNA PRXs sequences were PCR-amplified with AttB recombination sites. PCR products were then recombined first in pDONOR207 and transferred into pGWB83. To generate transcriptional reporter, the PRXs promoter regions (2Kb) was amplified and recombined first in pDONOR207 and transferred into pMDC111.

SS-TOM and SS-TOM-Long-EXT constructs. The binary vector pART27, encoding tdTomato secreted with the secretory signal sequence from tomato polygalacturonase and expressed by the constitutive CaMV 35S promoter (pART-SS-TOM), was the kind gift of Dr. Jocelyn Rose, Cornell University. The entire reporter protein construct was excised from pART-SS-TOM by digesting with *Not*I. The resulting fragments were gel-purified with the QIAquick Gel Extraction Kit and ligated using T4 DNA Ligase (New England Biolabs) into dephosphorylated pBlueScript KS+ that had also been digested with *Not*I and gel-purified to make pBS-SS-TOM. The plasmid was confirmed by sequencing with primers 35S-FP (5'-CCTTCGCAAGACCCTTCCTC-3') and OCS-RP (5'-CGTGCACAACAGAATTGAAAGC-3'). The sequence of the EXT domain from *SlPEX1* (NCBI accession AF159296) was synthesized and cloned by GenScript into pUC57 (pUC57-EXT). The plasmid pBS-SS-TOM-Long-EXT was made by digesting pUC57-EXT and pBS-SS-TOM with *Nde*I and *Sgr*AI, followed by gel purification of the 2243 bp band from pUC57-EXT and the 5545 bp band from pBS-SS-TOM, and ligation of the two gel-purified fragments. The pBS-SS-TOM-Long-EXT plasmid was confirmed by sequencing with 35S-FP, OCS-RP, and tdt-seq-FP (5'- CCCGTTCAATTGCCTGGT-3'). Both pBS plasmids were also confirmed by digestion. The binary vector pART-SS-TOM-Long-EXT was made by gel purifying the *Not*I insert fragment from the pBS-SS-TOM-Long EXT plasmid and ligating it with pART-

SS-TOM backbone that had been digested with *Not*I, gel purified, and dephosphorylated. This plasmid was confirmed by sequencing with 35S-FP, OCS-RP, and tdt-seq-FP.

Root hair phenotype. For quantitative analysis of root hair phenotypes in *PRX01,44,73* mutants, 35S:PRX-GFP lines and Wt Col-0, 200 fully elongated root hairs were measured (n roots= 20-30) from seedlings grown on vertical plates for 10 days. Values are reported as the mean ±SD using the Image J software. Measurements were made after 7 days. Images were captured with an Olympus SZX7 Zoom microscope equipped with a Q-Colors digital camera.

Confocal imaging. Root hairs were ratio imaged with the Zeiss LSM 710 laser scanning confocal microscope (Carl Zeiss) using a 40X oil-immersion, 1.2 numerical aperture. EGFP (473–505nm) emission was collected using a 458-nm primary dichroic mirror and the meta-detector of the microscope. Bright-field images were acquired simultaneously using the transmission detector of the microscope. Fluorescence intensity was measured in 7 µm ROI (Region Of Interest) at the root hair apex. For cytoplasmatic ROS measurements, samples were observed with a confocal microscope equipped with a 488-nm argon laser and BA510IF filter sets. A 10× objective was used, 0.30 N.A., 4.7 laser intensity, 1.1 offset, 440 photomultiplier (PMT) (for highest ROS levels), 480 PMT (for ROS media), and gain 3. Images were taken scanning XZY with 2 µm between focal planes. Images were analyzed using ImageJ. To measure $_{cyt}$ROS highest levels, a circular region of interest (ROI) (r = 2.5) was chosen in the zone of the root hair with the highest intensities. To measure ROS mean, the total area of the root hair was taken. To measure apoplastic ROPS, stained root hair cells were imaged with a Zeiss LSM5 Pascal laser scanning confocal microscope. The fluorescence emission of oxidized AUR in the apoplast of root hair cells was observed between 585 and 610 nm using 543 nm argon laser excitation, 40X objective, N/A= 1.2. Quantification of the AUR probing fluorescence signal was restricted to apoplastic spaces at the root hair tip.

Peroxidase activity. Soluble proteins were extracted from roots grown on agar plates in a Percival incubator at 22°C in a growth room for 10 days at 140 µmol $m^{-2}s^{-1}$ light intensity by grinding in 20mM HEPES, pH 7.0, containing 1 mM EGTA, 10mM ascorbic acid, and PVP PolyclarAT (100mg g^{-1} fresh material; Sigma, Buchs, Switzerland). The extract was centrifuged twice for 10 min at 10,000 g. Each extract was assayed for protein levels with the Bio-Rad assay (Bio-Rad). PRX activity was measured at 25°C by following the oxidation of 8 mM guaiacol (Fluka) at 470 nm in the presence of 2 mM H_2O_2 (Carlo Erba) in a phosphate buffer (200 mM, pH6.0). Values are the mean of three replicates ± SD.

ROS measurements. To measure cytoplasmic ROS ($_{cyt}$ROS) measurements in root hairs, seedlings were incubated in darkness on a slide for 10 min with 50 µM 2′,7′-dichlorodihydrofluorescein diacetate (H_2DCF-DA) at room temperature. Samples were observed with a confocal microscope. To

quantify apoplastic ROS ($_{apo}$ROS) levels in root hairs, levels of apoplastic H_2O_2 were measured using a solution of Amplex™ UltraRed Reagent (AUR, Molecular Probes). Briefly, Arabidopsis seedlings were incubated with 50 µM AUR for 20 min in dark conditions.

Phylogenetic analysis. 73 class-III PRX protein sequences from *A. thaliana*, two putative lignin class-III PRXs from *Zinnia elegans* and 4 putative Extensin class-III PRXs from *Lupinus album*, *Lycopersicum esculentum*, *Phaseolus vulgaris* and *Vitis vinifera*, have been aligned with ClustalW and the tree constructed using the Neighbor-Joining method (Saitou and Nei, 1987). The analyses were conducted in MEGA7 (Kumar, 2016). All protein sequences are available using their ID number (http://peroxibase.toulouse.inra.fr (Savelli et al., 2019).

Co-expression analysis network. Co-expression networks for *RSL4* root hair genes were identified from PlaNet (http://aranet.mpimp-golm.mpg.de) and trimmed to facilitate readability (Mutwill et al. 2011). Each co-expression of interest was confirmed independently using the expression angler tool from Botany Array Resource BAR (http://bar.utoronto.ca/ntools/cgi-bin/ntools_expression_angler.cgi) and ATTED-II (http://atted.jp). Only those genes that are connected with genes of interest are included.

Tyr-crosslinking analysis. Alcohol-insoluble residues of root tissues obtained from *PRX01,44,73* mutants, Col-0 and 35S:PRX-GFP lines were hydrolyzed in 6 N HCl (aqueous) with 10 mM phenol (2 mg ml^{-1}; 110 °C; 20 h). Hydrolysates were dried under a steady stream of nitrogen (gas) and then re-dissolved at 10 mg ml^{-1} in water. The hydrolysates were fractionated by gel permeation chromatography on a polyhydroxyethyl A column (inner diameter, 9.4 x 200 mm, 10 nm pore size, Poly LC Inc., Columbia, MD) equilibrated in 50 mM formic acid and eluted isocratically at a flow rate of 0.8 ml min^{-1}. UV absorbance was monitored at 280 nm. The amounts of Tyr and IDT in the hydrolysates were then determined by comparison with peak areas of authentic Tyr and IDT standards. Response factors were determined from three level calibrations with the Tyr and IDT standards.

Immuno-blot Analysis. Plant material (100 mg of root from 15 days old seedlings grown as indicated before) was collected in a microfuge tube and ground in liquid nitrogen with 400 mL of protein extraction buffer (125 mM Tris-Cl, pH. 4.4, 2% [w/v] SDS, 10% [v/v] glycerol, 6M UREA, 1% [v/v] b-mercaptoethanol, 1mM PMSF). Samples were immediately transferred to ice. After 4° centrifugations at 13000 rpm for 20 min, supernatant was move to a new 1.5 ml tube and equal volumes of Laemmli buffer (125 mM Tris-Cl, pH. 7.4, 4% [w/v] SDS, 40% [v/v] glycerol, 10% [v/v] b-mercaptoethanol, 0.002% [w/v] bromphenol blue) were added. The samples (0.5–1.0 mg/mL of protein) were boiled for 5 min and 30 mL were loaded on 10% SDS-PAGE. The proteins were separated by electrophoresis and transferred to nitrocellulose membranes. Anti-GFP mouse IgG

(clones 7.1 and 13.1; Roche Applied Science) was used at a dilution of 1:2,000 and it was visualized by incubation with goat anti-mouse IgG secondary antibodies conjugated to horseradish peroxidase (1:2,000) followed by a chemiluminescence reaction (Clarity Western ECL Substrate; Bio-rad). For the SS-TOM lines analysis, proteins were extracted in 2x SDS buffer (4% SDS, 125mM Tris pH 6.8, 20% glicerol, 0.01% bromofenol blue, 50 mM ditiotreitol [DTT]), using 10 µl of buffer per mg of plant tissues of Wt Col-0, transgenic lines 35S:SS-TOM and 35S:SS-TOM-Long-EXT. Two transgenic lines were analyzed. 10 µl of supernatant of each protein extract were run into a 12% poliacrilamide gel during one hour at 200 V, and then transferred to a PVDF membrane. PVDF was blocked with 5% milk in TBST (Tris-HCl 10 mM, pH 7,4, NaCl 150 mM, Tween-20 al 0,05%) for 1 hour at 4ºC and then washed four times during 15 min in TBST. An anti-RFP (A00682, GenScript) was used as primary antibody overnight at 4ºC. Four washes of 15 min each in TBST at r.t. and then it was incubated two hours with a secondary antibody anti-rabbit (goat) conjugated with alkaline phosphatase (A3687, Sigma), in a 1:2,500 dilution with TBST. Four washes of 15 min each in TBST at room temperature. Finally, 10 ml of alkaline phosphatase (100mM Tris-HCl pH 9.5, 100 mM NaCl, 3 mM MgCl2) containing 80 µl NBT (Sigma) (35mg/ml in70% DMSO and 30 µl de BCIP (Sigma) (50 mg/ml in 100% de DMSO) were used.

Transmission electron microscopy of root hair cell walls. Seeds were germinated on 0.2x MS, 1% sucrose, 0.8% agar. Seven days after germination, seedlings were transferred to new 0.2x MS, 1% sucrose, 0.8% agar plates with or without 100 µM SHAM. After 4 additional days, 1-mm root segments with root hairs were fix in 2% glutaraldehyde in 0.1M cacodylate buffer pH7.4. Samples were rinsed in cacodylate buffer and post-fixed in 2% OsO4. After dehydration in ethanol and acetone, samples were infiltrated in Epon resin (Ted Pella, Redding, CA). Polymerization was performed at 60°C. Sections were stained with 2% uranyl acetate in 70% methanol followed by Reynold's lead citrate (2.6% lead nitrate and 3.5% sodium citrate [pH 12.0]) and observed in a Tecnai 12 electron microscope. Quantitative analysis of cell wall thickness was performed using FIJI.

Modeling and molecular docking between PRXs and EXTs. Modeling and molecular docking: cDNA sequences of PRXs were retrieved from TAIR (PRX01: AT1G05240, PRX36: AT3G50990, PRX44: AT4G26010, PRX64: AT5G42180, PRX73: AT5G67400) and NCBI Nucleotide DB (PRX24Gv:Vitis vinifera peroxidase 24, GvEP1, LOC100254434). Homology modeling was performed for all PRXs using modeller 9.14 (Sali et al. 1993), using the crystal structures 1PA2, 3HDL, 1QO4 and 1HCH as templates, available at the protein data bank. 100 structures where generated for each protein and the best scoring one (according to DOPE score) was picked. The *receptor* for the docking runs was generated by the prepare_receptor4 script from autodock suite, adding hydrogens and constructing bonds. Peptides based on the sequence PYYSPSPKVYYPPPSSYVYPPPPS were used, replacing proline by hydroxyproline, and/or adding *O*-Hyp glycosylation with up to four arabinoses per hydroxyproline in the fully glycosylated peptide and a galactose on the serine, as it is usual in plant *O*-Hyp

https://www.ncbi.nlm.nih.gov/pmc/articles/PMC5045529/. Ligand starting structure was generated as the most stable structure by molecular dynamics (Velasquez et al. 2015a). All ligand bonds were set to be able to rotate. Docking was performed in two steps, using Autodock vina (Trott et al. 2010). First, an exploratory search over the whole protein surface (exhaustiveness 4) was done, followed by a more exhaustive one (exhaustiveness 8), reducing the search space to a 75x75x75 box centered over the most frequent binding site found in the former run.

EXT conformational coarse-grained model. The use of coarse-grained (CG) molecular dynamics (MD) allowed collection of long timescale trajectories. System reduction is significant when compared to all atom models, approximately reducing on order of magnitude in particle number. In addition, a longer integration time step can be used. Protein residues and coarse grained solvent parameters correspond to the SIRAH model (Darré et al. 2015), while ad hoc specific glycan parameters were developed. The CG force field parameters developed correspond to arabinofuranose and galactopyranose (**Figure S5**). Triple helix systems were simulated both, in the non-glycosylated and fully *O*-glycosylated states, where all the hydroxyprolines are bound to a tetrasaccharide of arabinofuranoses, and specific serine residues contain one galactopyranose molecule. They were immersed in WT4 GC solvent box that was constructed to be 2 nm apart from the extensin fiber, and periodic boundary conditions were employed. Coarse grained ions were also included to achieve electroneutrality and 0.15 M ionic strength. All simulations were performed using the GROMACS MD package at constant temperature and pressure, using the Berendsen thermostat (respectively) and Parrinello-Rahman barostat (Parrinello and Rahman 1981), and a 10 fs time step. The obtained trajectories were analysed using the Mdtraj python package (McGibbon et al, 2015) and visualized with Visual Molecular Dynamics (VMD) 1.9.1 (Humphrey et al. 1996). Volume measurements were performed using a Convex Hull algorithm implemented in NumPy (Oliphant 2006), and average diameter calculations were derived from this quantity using simple geometric arguments.

Acknowledgements

We thank Andres Rossi from the microscopy facility of FIL for his assistance. We thank ABRC (Ohio State University) for providing T-DNA lines seed lines. J.M.E. is Principal Investigator of the National Research Council (CONICET) from Argentina. This work was supported by grants from ANPCyT (PICT2016-0132 and PICT2017-0066) and a grant from ICGEB CRP/ARG16-03 to J.M.E. In addition, this research is also funded by Instituto Milenio iBio – Iniciativa Científica Milenio, MINECON to J.M.E. and NSF MCB grant 1614965 to M.S.O.

Author Contribution

E.M and C.B performed most of the experiments and analysed the data. P.R. and C.D. analysed the peroxidase activity and performed phylogenetic analysis. J.W.M-E and M.H. analysed the Tyr-crosslinking on EXTs. A.A.A. and A.D.N performed the docking experiments and analysed this data. M.B. and L.C. perform the EXT modelling and analysed this data. M.F. and P.B generated the EXT reporter lines and performed the immune-blots analysis of SS-TOM and SS-TOM-Long-EXT lines. J.M.P., D.R.R.G., Y.d.C.R.G., S.M., and F.B.H. analysed the data. J.P., J.P-V., and M.S.O. performed the transmission electron microscopy analysis. J.M.E. designed research, analysed the data, supervised the project, and wrote the paper. All authors commented on the results and the manuscript. This manuscript has not been published and is not under consideration for publication elsewhere. All the authors have read the manuscript and have approved this submission.

Competing financial interest

The authors declare no competing financial interests. Correspondence and requests for materials should be addressed to J.M.E. (Email: jestevez@leloir.org.ar / jose.estevez@unab.cl).

REFERENCES

Baumberger N, Ringli C, Keller B. (2001). The chimeric leucine rich repeat/extensin cell wall protein LRX1 is required for root hair morphogenesis in *Arabidopsis thaliana*. *Genes & Development* 15, 1128–1139.

Baumberger N, Steiner M, Ryser U, Keller B, Ringli C. (2003). Synergistic interaction of the two paralogous Arabidopsis genes LRX1 and LRX2 in cell wall formation during root hair development. *Plant J.* 35, 71–81.

Berendsen, H. J. C., Postma, J.P.M., van Gunsteren, W.F., DiNola, A., and Haak, J.R. (1984) Molecular dynamics with coupling to an external bath. *J. Chem. Phys.* 81, 3684. doi: 10.1063/1.448118.

Berman HM, John Westbrook, Zukang Feng, Gary Gilliland, Talapady N Bhat, Helge Weissig, Ilya N Shindyalov, and Philip E Bourne. The protein data bank. *Nucleic Acids Research*, 28(1):235–242, 2000.

Bernards, M.A., Fleming, W.D., Llewellyn, D.B., Priefer, R., Yang, X., Sabatino, A., and Plourde, G.L. (1999). Biochemical characterization of the suberization-associated anionic peroxidase of potato. *Plant Physiol.* 121: 135–146.

Bhave G, Cummings CF, Vanacore RM, Kumagai-Cresse C, Ero-Tolliver IA, Rafi M, Kang J-S, Pedchenko V, Fessler LI, Fessler JH, Hudson BG (2012) Peroxidasin forms sulfilimine chemical bonds using hypohalous acids in tissue genesis. *Nat. Chem. Biol.* 8:784–790.

Brady, J.D., Sadler, I.H., and Fry, S.C. (1996). Di-isodityrosine, a novel tetrametric derivative of tyrosine in plant cell wall proteins: a new potential cross-link. *Biochem. J* 315: 323–327.

Brady, J.D., Sadler, I.H., and Fry, S.C. (1998). Pulcherosine, an oxidatively coupled trimer of tyrosine in plant cell walls: its role in cross-link formation. *Phytochemistry*. 47(3):349-353.

BrownK.L, C.F. Cummings, R.M. Vanacore and B.G. Hudson. (2017). Building collagen IV smart scaffolds on the outside of cells. *Protein Sci.* 26:2151-2161.

Brownleader, M.D., Ahmed, N., Trevan, M., Chaplin, M.F., and Dey, P.M. (1995). Purification and partial characterization of Tomato extensin peroxidase. *Plant Physiol.* 109: 1115–1123

Cannon, M.C., Terneus, K., Hall, Q., Tan, L., Wang, Y., Wegenhart, B.L., Chen, L., Lamport, D.T., Chen, Y., and Kieliszewski, M.J. (2008). Self-assembly of the plant cell wall requires an extensin scaffold. *Proc. Natl. Acad. Sci. USA*. 105: 2226–2231.

Chen, Y., Dong, W., Tan, L., Held, M. A., & Kieliszewski, M. J. (2015). Arabinosylation plays a crucial role in extensin cross-linking in vitro. *Biochemistry insights*, *8*, BCI-S31353.

Cosio C. & Dunand C. (2009). Specific functions of individual class III peroxidases genes. *J. Exp. Bot.* 62:391–408.

Cosio C., Ranocha Ph., Francoz E., Burlat V., Zheng Y., Perry S.E., Ripoll J.-J., Yanofsky M., Dunand C. (2017) The class III peroxidase PRX017 is a direct target of the MADS-box transcription factor 1 AGL15 and participates in lignified tissue formation. *New Phytol*. 213: 250-263.

Darré, L., Machado, M.R., Brandner, A.F., González, H.C., Ferreira, S., and Pantano, S. (2015). SIRAH: A structurally unbiased coarse-grained force field for proteins with aqueous solvation and long-range electrostatics. *J. Chem. Theory Comput.* 11(2):723–739

Dong, W., Kieliszewski, M., and Held, M.A. (2015). Identification of the pI 4.6 extensin peroxidase from *Lycopersicon esculentum* using proteomics and reverse-genomics. *Phytochem.* 112:151–159.

591 Dunand, C., Crevecoeur, M., and Penel, C. (2007). Distribution of superoxide and hydrogen peroxide
592 in Arabidopsis root and their influence on root development: possible interaction with
593 peroxidases. *New Phytol*. 174:332–341.
594 Francoz et al. (2019) Pectin demethylesterification generates platforms that anchor peroxidases to
595 remodel plant cell wall domains. *Developmental Cell* 48, 1-16.
596 Held, M. A., Tan, L., Kamyab, A., Hare, M., Shpak, E., and Kieliszewski, M. J. (2004). Di-isodityrosine is
597 the intermolecular cross-link of isodityrosine-rich extensin analogs cross-linked in vitro. *Journal*
598 *of Biological Chemistry*, *279*(53), 55474-55482.
599 Humphrey, W., Dalke, A., and Schulten, K. (1996). VMD: Visual molecular dynamics. *J. Molec.*
600 *Graphics* 14:33-38
601 Jackson, P.A., Galinha, C.I., Pereira, C.S., Fortunato, A., Soares, N.C., Amâncio, S.B., and Pinto
602 Ricardo, C.P. (2001). Rapid deposition of extensin during the elicitation of grapevine callus
603 cultures is specifically catalyzed by a 40-kilodalton peroxidase. *Plant Physiol.* 127: 1065–1076.
604 Jacobowitz, J.R, Doyle W.C., and Weng, J-K. (2019). PRX9 and PRX40 are extensin peroxidases
605 essential for maintaining tapetum and microspore cell wall integrity during Arabidopsis anther
606 development. *Plant Cell* 31: 848–86.
607 Kim D Pruitt, Tatiana Tatusova, and Donna R Maglott. Ncbi reference sequences (refseq): a curated
608 non-redundant sequence database of genomes, transcripts and proteins. *Nucleic Acids Research*,
609 35(suppl 1):D61–D65, 2006.
610 Kumar, S., Stecher G., Tamura K. (2016) MEGA7: molecular evolutionaary genetic analysis version
611 7.0 for bigger datasets. *Mol. Biol. Evol.* 33(7): 1870-1874.
612 Lamport, D.T.A., Kieliszewski, M.J., Chen, Y., and Cannon, M.C. (2011). Role of the extensin
613 superfamily in primary cell wall architecture. *Plant Physiol*. 156: 11–19.
614 Lee, Y., Rubio, M.C., Alassimone, J., and Geldner, N. (2013). A mechanism for localized lignin
615 deposition in the endodermis. *Cell* 153: 402–412.
616 Mangano S. *et al.* (2017). The molecular link between auxin and ROS-controlled root hair growth.
617 *Proc. Natl. Acad. Sci. U.S.A*. 114(20):5289-5294.
618 Marzol E, Borassi C, Bringas M, Sede A, Rodríguez Garcia DR, Capece L, Estevez JM. (2018). Filling the
619 Gaps to Solve the Extensin Puzzle. *Mol Plant*. 11(5):645-658.
620 McGibbon R.T, Beauchamp K.A., Harrigan M.P., Klein C., Swails, J.M., Hernández C.X., Schwantes
621 C.R., Wang, L.P., Lane T.J., Pande V.S. (2015) MDTraj: A Modern Open Library for the Analysis of
622 Molecular Dynamics Trajectories. *Biophysical Journal*, 109(8): 1528-1532
623 Mutwil, M., Klie, S., Tohge, T., Giorgi, F.M., Wilkins, O., Campbell, M.M., Fernie, A.R., Usadel, B.,
624 Nikoloski, Z. and Persson, S. (2011). PlaNet: combined sequence and expression comparisons
625 across plant networks derived from seven species. *Plant Cell*, 23, 895– 910.
626 Oliphant, TE. USA: Trelgol Publishing, (2006). A guide to NumPy. 376 pp.
627 Parrinello, M. and Rahman, A. *(1981).* Polymorphic transitions in single crystals: A new molecular
628 dynamics method. *J. of Applied Physics* 52:7182. doi.org/10.1063/1.328693
629 Passardi, F., Penel, C., and Dunand, C. (2004). Performing the paradoxical: how plant peroxidases
630 modify the cell wall. *Trends Plant Sci*. 9:534–540.
631 Pereira S.P., J.M.L. Ribeiro, A.D. Vatulescu, K. Findlay, A.J. MacDougall and P.A.P. Jackson. (2011)
632 Extensin network formation in *Vitis vinifera* callus cells is an essential and causal event in rapid
633 and H_2O_2-induced reduction in primary cell wall hydration. *BMC Plant Biology* 111:106-121.

Price, N.J., Pinheiro, C., Soares, C.M., Ashford, D.A., Ricardo, C.P., and Jackson, P.A. (2003). A biochemical and molecular characterization of LEP1, an extensin peroxidase from lupin. *J. Biol. Chem.* 278:41389–41399.

Ringli C. (2010). The hydroxyproline-rich glycoprotein domain of the Arabidopsis LRX1 requires Tyr for function but not for insolubilization in the cell wall. *Plant J.* 63, 662–669.

Saitou N, Nei M. (1987). The neighbor-joining method: a newmethod for reconstruction of phylogenetic trees. Mol Biol Evol4:406–25.

Šali A., and Tom L Blundell. (1993). Comparative protein modelling by satisfaction of spatial restraints. *J. of Molecular biology*, 234(3):779–815.

Savelli B., Li Q., Webber M., Jemmat A.M., Robitaille A., Zamocky M., Mathe C., Dunand C. (2019). RedoxiBase a database for ROS homeostasis regulated proteins. *Redox Biol.* doi.org/10.1016/j.redox.2019.101247.

Schnabelrauch, L.S., Kieliszewski, M., Upham, B.L., Alizedeh, H., and Lamport, D. (1996). Isolation of pI 4.6 extensin peroxidase from tomato cell suspension cultures and identification of Val-Tyr-Lys as putative intermolecular cross-link site. *Plant J.* 9:477–489.

Sede, A.R., Borassi, C., Wengier, D.L., Mecchia, M.A., Estevez, J.M., and Muschietti, J.P. (2018). Arabidopsis pollen extensins LRX are required for cell wall integrity during pollen tube growth. *FEBS Lett.* 592, 233–243.

Shen Y., Rosendale M., Campbell R.E., D. Perrais (2014). pHuji, apH-sensitive red fluorescent protein for imaging of exo- and endocytosis. *J.Cell Biol.* 207 (3):419-432.

Smith, A.T., Santama, N., Dacey, S., Edwards, M., Bray, R.C., Thorneley, R.N., and Burke, J.F. (1990). Expression of a synthetic gene for horseradish peroxidase C in *Escherichia coli* and folding and activation of the recombinant enzyme with Ca^{2+} and heme. *J. Biol. Chem.* 265: 13335–13343.

Stoddard, A and Rolland, V. (2018). I see the light!. Fluorescent proteins suitable for the cell wall/apoplat targeeting in *Nicotiana benthamiana* leaves. *Plant Direct.* doi.org/10.1002/pld3.112

Strasser, R. (2016). Plant protein glycosylation. *Glycobiology*. 26(9):926–939.

Stratford, S., et al. (2001). A leucine-rich repeat region is conserved in pollen extensin-like (Pex) proteins in monocots and dicots. *Plant Mol. Biol.* 46:43–56.

Trott O., and Arthur J Olson. (2010). Autodock vina: improving the speed and accuracy of docking with a new scoring function, efficient optimization, and multithreading. *Journal of Computational Chem.* 31(2):455–461.

Vanacore R, Ham AJ, Voehler M, Sanders CR, Conrads TP, Veenstra TD, Sharpless KB, Dawson PE, Hudson BG (2009) A sulfilimine bond identified in collagen IV. Science 325:1230–1234.

Velasquez, S.M., Ricardi, M.M., Dorosz, J.G., Fernandez, P.V., Nadra, A.D., Pol-Fachin, L., Egelund, J., Gille, S., Ciancia, M., Verli, H., et al. (2011). O-glycosylated cell wall extensins are essential in root hair growth. *Science* 332:1401–1403.

Velasquez M, Salter JS, Dorosz JG, Petersen BL, Estevez JM. (2012). Recent advances on the posttranslational modifications of EXTs and their roles in plant cell walls. *Frontiers in plant science* 3, 93.

Velasquez SM, Marzol E, Borassi C, Pol-Fachin L, Ricardi MM, Mangano S, Denita JS, Salgado SJ, Gloazzo DJ, Marcus SE. (2015a). Low sugar is not always good: Impact of specific O-glycan defects on tip growth in Arabidopsis. *Plant Physiology* 168, 808–813.

676 Velasquez, S.M., Ricardi, M.M., Poulsen, C.P., Oikawa, A., Dilokpimol, A., Halim, A., Mangano, S.,
677 Denita-Juarez, S.P., Marzol, E., Salgoda Salter, J.D., et al. (2015b). Complex regulation of prolyl-4-
678 hydroxylases impacts root hair expansion. *Mol. Plant* 8:734–746.
679 Wang, X., Wang, K., Yin, G., Liu, X., Liu, M., Cao, N., Duan, Y., Gao, H., Wang, W., Ge, W., et al.
680 (2018). Pollen-expressed leucine-rich repeat extensins are essential for pollen germination and
681 growth. *Plant Physiol*. 176, 1993–2006.
682 Wojtaszek, P., Trethowan, J., and Bolwell, G.P. (1997). Reconstitution in vitro of the components and
683 conditions required for the oxidative cross-linking of extracellular proteins in French bean
684 (Phaseolus vulgaris L.). *FEBS Lett.* 405:95–98.
685 Yi K, Menand B, Bell E, Dolan L. (2010). A basic helix-loop-helix transcription factor controls cell
686 growth and size in root hairs. *Nature genetics* 43: 264-267.

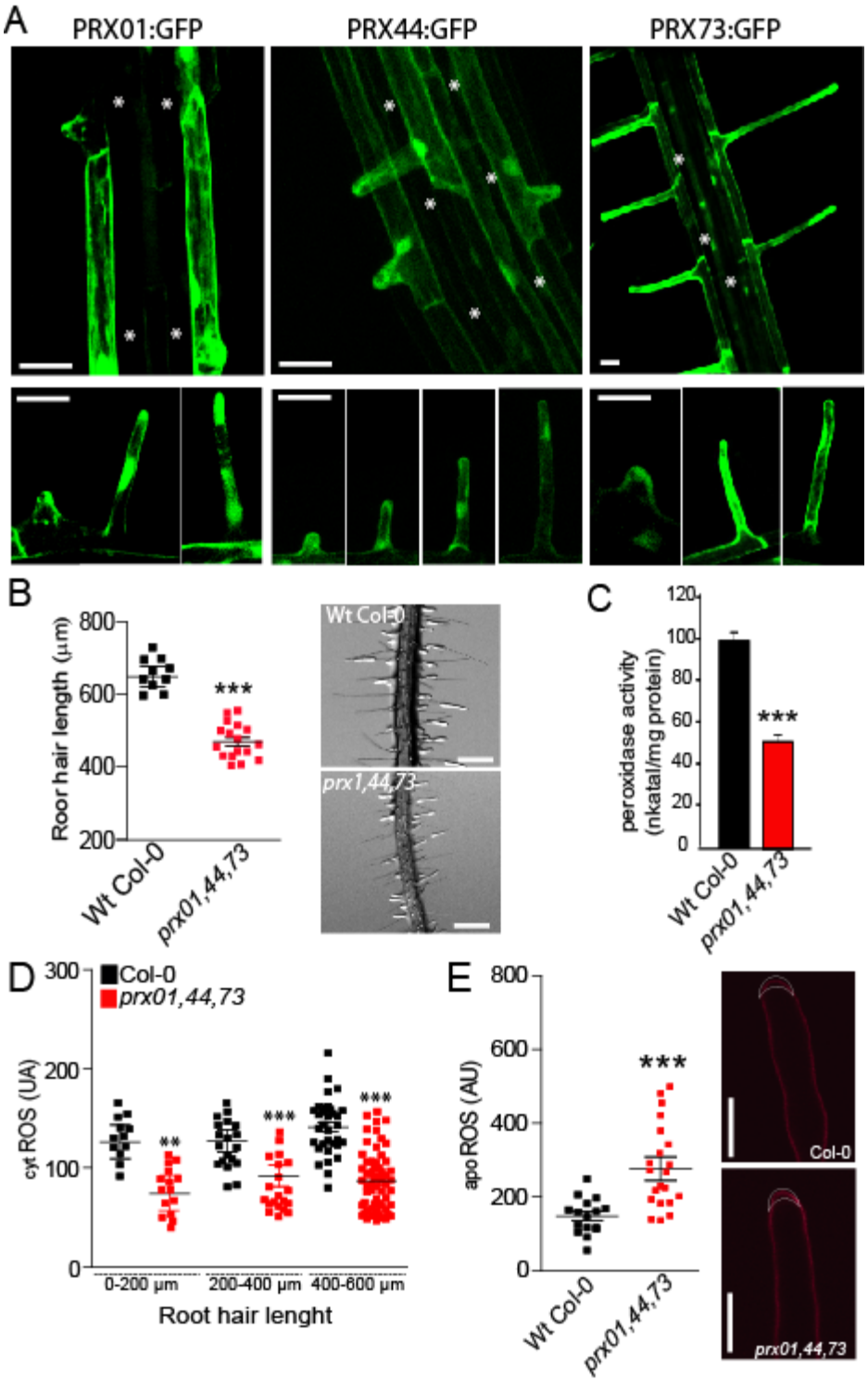

687
688

689 **Figure 1. Characterization of root hair-specific PRX01, PRX44 and PRX73 expression and mutant**
690 **analysis.**

(**A**) GFP-tagged transcriptional reporters of PRX01, PRX44 and PRX73 show expression in the root elongation zone and specifically in root hairs (bottom). Scale bar = 20 µm. (*) indicates atrichoblast cell layers, which lack GFP expression.

(**B**) Root hair length phenotype of Wt and the *prx01,44,73* triple mutant. Left, box-plot of root hair length. Horizontal lines show the means. P-value determined by one-way ANOVA, (***) P<0.001. Right, bright-field images exemplifying the root hair phenotype in each genotype. Scale bars, 1 mm.

(**C**) Peroxidase activity in Wt and *prx01,44,73* triple mutant roots. Enzyme activity values (expressed as nkatal/mg protein) are shown as the mean of three replicates ± SD. P-value determined by one-way ANOVA, (***) P<0.001.

(**D**) Cytoplasmic ROS levels measured with H_2DCF-DA in Wt and *prx01,44,73* triple mutant root hairs. Horizontal lines show the means. P-values determined by one-way ANOVA, (***) P<0.001 and (**) P<0.01.

(**E**) Apoplastic ROS levels measured with Amplex™ UltraRed (AUR) in Wt and *prx01,44,73 73* triple mutant root hairs. ROS signal was quantified from the root hair cell tip. Left, box-plot of apoROS values. Horizontal lines show the means. P-value determined by one-way ANOVA, (***) P<0.001. Right, fluorescence images exemplifying apoROS detection in root hair apoplast.

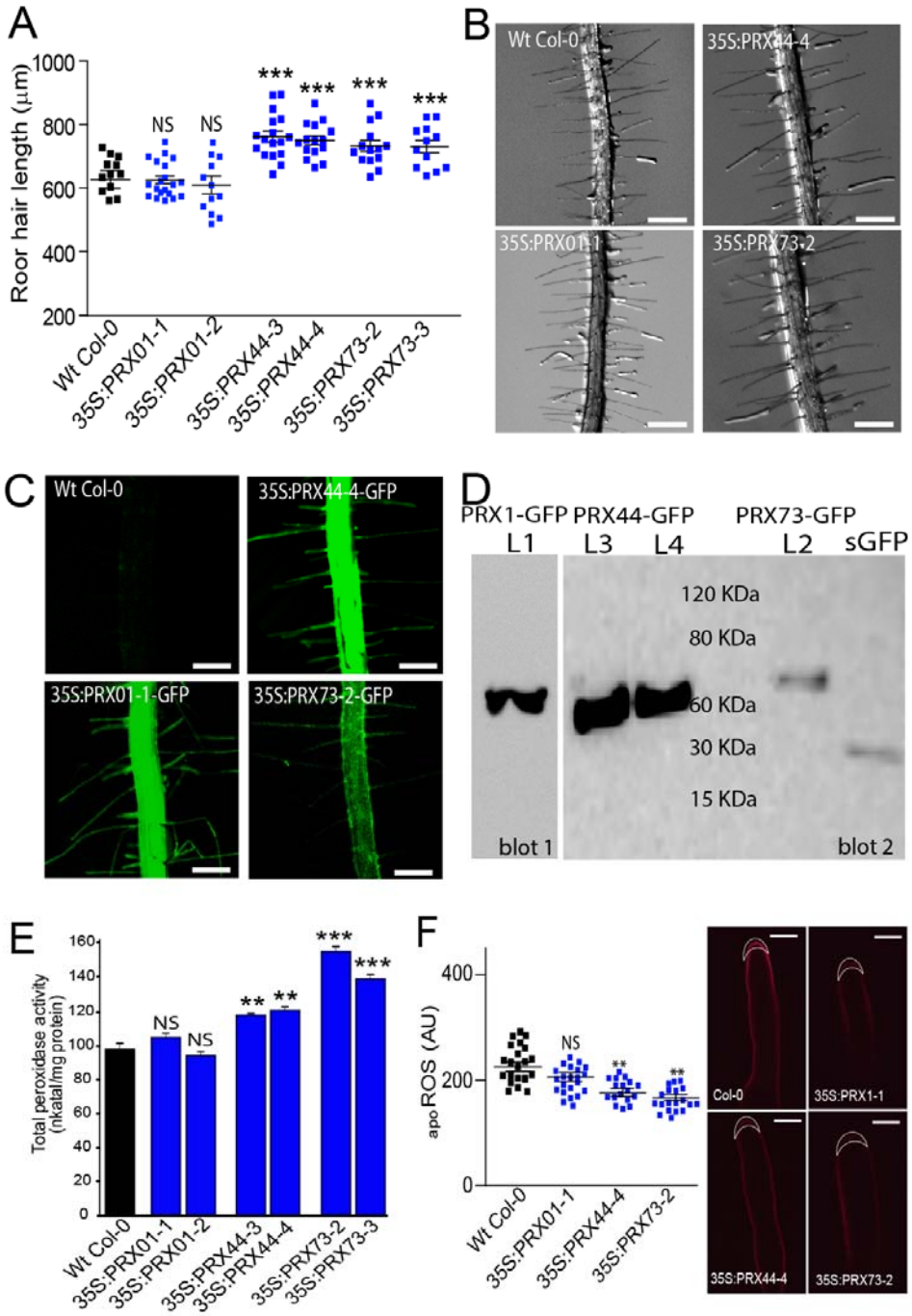

Figure 2. Over-expression of PRX44 and PRX73 promotes root hair growth and higher root peroxidase activity.

(**A**) Root hair length phenotype of Wt and PRX^{OE} lines (in Wt background). Box-plot of root hair length. Horizontal lines show the means. P-values determined by one-way ANOVA, (***) P<0.001, (NS) not significantly different.

(**B**) Bright-field images exemplifying the root hair phenotype analyzed in Figure 2A. Scale bar = 0.5 mm.

(**C**) Expression of GFP-tagged 35S:PRX01, 35S:PRX44 and 35S:PRX73 in root hair cells.

(**D**) Western blot of PRX01-GFP, PRX44-GFP and PRX73-GFP. Soluble GFP (sGFP) was used as control. The predicted molecular weights are 62.6 KDa for PRX01-GFP, 60.8 KDa for PRX44-GFP, 62.9 KDa for PRX73 and 27 KDa for sGFP.

(**E**) Assays of total peroxidase activity in Wt and PRXs^{OE} lines (in Wt background). Enzyme activity (expressed in nkatal/mg protein) was determined by a guaiacol oxidation-based assay. Values are the mean of three replicates ± SD. P-values determined by one-way ANOVA, (***) P<0.001, (**) P<0.01, (NS) not significantly different.

(**F**) Apoplastic ROS levels measured with Amplex™ UltraRed (AUR) in Wt and PRX^{OE} lines (in Wt background). ROS signal was quantified from the root hair cell tip. Left, box plot of apoROS values. Horizontal lines show the means. P-values determined by one-way ANOVA, (**) P<0.01, (NS) not significantly different. Right, fluorescence images exemplifying apoROS detection in root hair apoplast. Scale bar = 10 µm.

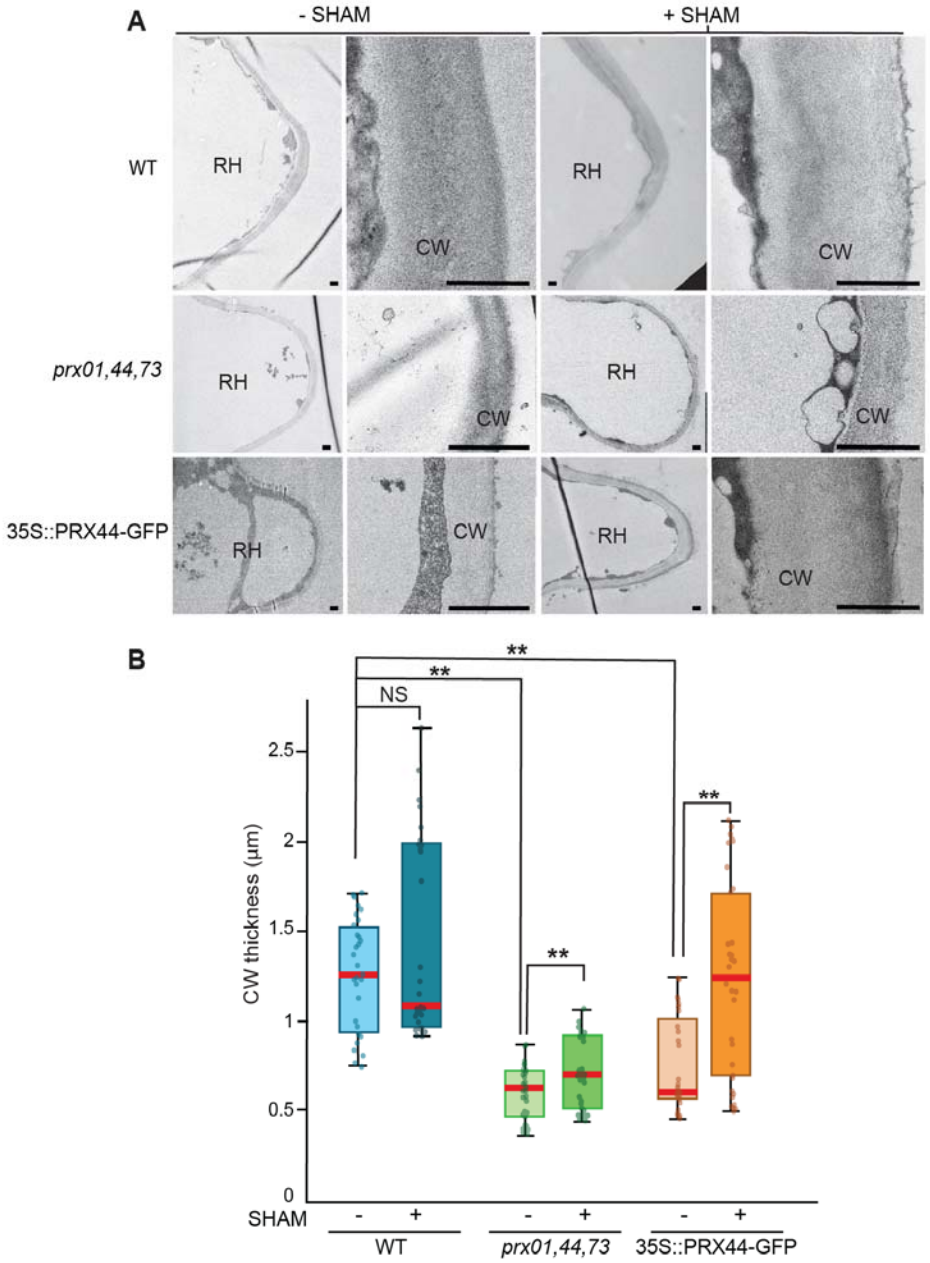

Figure 3. Effect of PRX expression on cell wall thickness in root hair tips.

(**A**) Transmission electron micrographs of root hair tips from Wt, *prx1,44,73* triple mutant, and PRX44^{OE} with (+) and without (-) peroxidase inhibitor SHAM. For each genotype and treatment, a representative overview of a root hair (RH) and a detail of the cell wall at the root hair tip (CW) is shown. Scale bar = 1 µm.

(**B**) Box and whisker plot showing cell wall thickness measured at the root hair tip of the three genotypes with or without SHAM treatment. (**) P□0.001 determined by t-test. (NS) not significantly different.

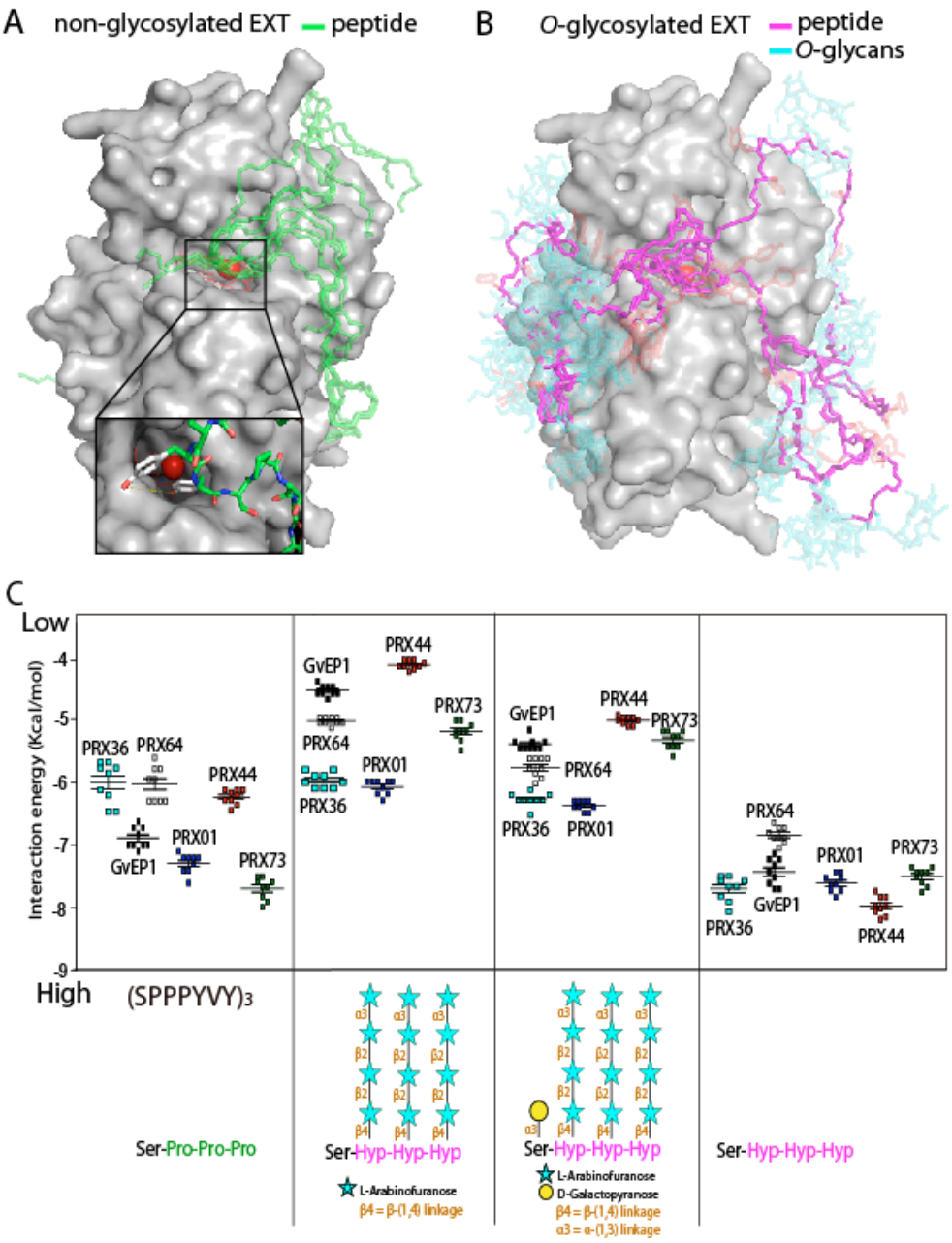

Figure 4. Interaction by an *in silico* docking approach of PRX01, PRX44 and PRX73 with EXT peptides.

(**A,B**) Ten docking results for each EXT *O*-glycosylation state are shown superimposed on the PRX44 protein surface to evaluate the consistence of docking sites.

(**A**) Model of PRX44 (protein surface shown in gray) complexed to a non-*O*-glycosylated EXT substrate $(SPPPYVY)_3$ (in green, depicted as sticks). Heme is depicted as thin sticks while iron is a red sphere. Bottom inset, two close tyrosine residues dock near to the possible active site of PRX44.

(**B**) Model of PRX44 (protein surface shown in gray) complexed to an *O*-glycosylated-EXT substrate (protein backbone shown in magenta, and *O*-glycans shown in light blue, both depicted as sticks). Heme is depicted as thin sticks while iron is a red sphere. Arabino-galactosylated EXT peptide = [$(SOOOYVY)_3$-AG].

(**C**) Comparison of the binding energy of different peroxidases to EXT substrates with different degrees of *O*-glycosylation. A non-hydroxylated EXT peptide $(SPPPYVY)_3$, a hydroxylated but not *O*-glycosylated EXT peptide [$(SOOOYVY)_3$; O=hydroxyproline], only arabinosylated EXT-peptide [$(SOOOYVY)_3$-A], and arabino-galactosylated EXT peptide [$(SOOOYVY)_3$-AG] were analyzed.

Table 1. Peptidyl-Tyr and iso-dityrosine (IDT) contents in cell walls isolated from Wt, *prx01,44,73* triple mutant, PRX^{OE} lines and mutant lines with under-glycosylated EXTs. P-values were determined by one-way ANOVA, (***) P≤0.001, (**) P≤0.01. STD=Standard Deviation. Values significantly different than Wt are highlighted in blue if higher and in light blue if lower than Wt Col-0.

	ng Tyr/µg CW (STD)	ng IDT/µg CW (STD)
Wt Col-0	7.799 ± 0.26	0.853 ± 0.08
prx01 prx44 prx73	9.588 ± 0.31**	0.963 ± 0.02
PRX44^{OE}	8.649 ± 0.07	0.953 ± 0.04
PRX73^{OE}	8.700 ± 0.12	1.042 ± 0.02**
under O-glycosylated EXTs		
sergt1-1 rra3	3.530 ± 0.08***	0.235 ± 0.01***
p4h5 sergt1-1	3.766 ± 0.06***	0.225 ± 0.02***

762 **Supplementary Information**

763

764 **Class III peroxidases PRX01, PRX44, and PRX73 potentially target extensins during root hair**
765 **growth in *Arabidopsis thaliana***

766

767

768 Eliana Marzol, Cecilia Borassi, Philippe Ranocha, Ariel. A. Aptekman, Mauro Bringas, Janice
769 Pennington, Julio Paez-Valencia, Javier Martínez Pacheco, Diana Rosa Rodríguez Garcia, Yossmayer
770 Rondon, Mariana Carignani, Silvina Mangano, Margaret Fleming, John W. Mishler-Elmore, Francisca
771 Blanco-Herrera, Patricia Bedinger, Christophe Dunand, Luciana Capece, Alejandro D. Nadra, Michael
772 Held, Marisa Otegui & José M. Estevez

773

774

775 † Correspondence should be addressed. Email: jestevez@leloir.org.ar / jose.estevez@unab.cl
776 (J.M.E).

777

778

779 The following Supporting Information is available for this article:
780 Supplementary Figures S1-S7
781 Supplementary Table S1
782 Supplementary References 6

783 **Table S1**. Volume and average diameter measurements of EXTs from molecular dynamics
784 simulations. These magnitudes were measured in the fully extended EXT system. Values shown are
785 the mean ± standard deviation.
786

	Non-glycosylated EXT	***O*-glycosylated EXT**	***O*-glycosylated EXT (protein only)**
Volume /nm^3	280 ± 30	1080 ± 50	450 ± 30
EXT length /nm	65 ± 2	70 ± 2	70 ± 2
Average diameter /nm	2.4	4.5	2.9
Distance Tyr-Tyr			
0-5 Å	20%	25%	-
5-7 Å	55%	65%	-

787

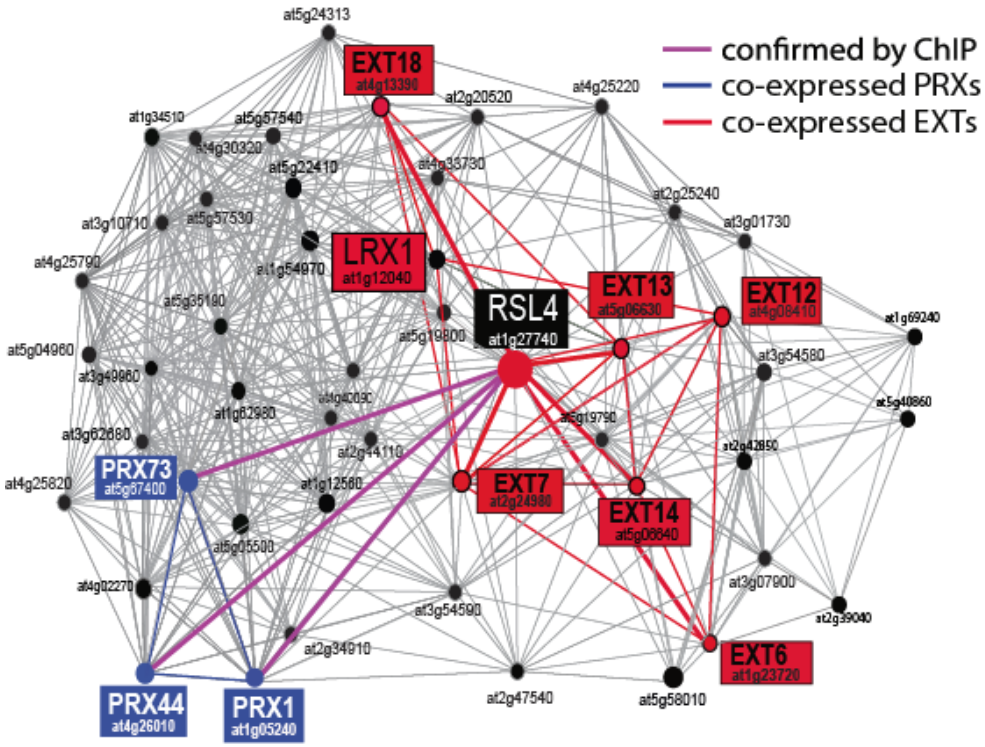

Figure S1. Root hair transcriptional co-expression network. PRXs, EXTs, and the transcriptional regulator RSL4 are highlighted. RSL4 was used as gene bait to narrow down the number of co-expressed genes. Transcriptional connections between RSL4 (in black), EXTs (in red) and PRXs genes (in blue). The co-expression network was identified from PLaNet (http://aranet.mpimp-golm.mpg.de/aranet) (Mutwil et al., 2011) and trimmed to facilitate readability. Chromatin immunoprecipitation assay (ChiP) showed that RSL4 binds and controls the expression of PRX01,44,73 (Mangano et al. 2017). Figure modified from Marzol et al. (2018).

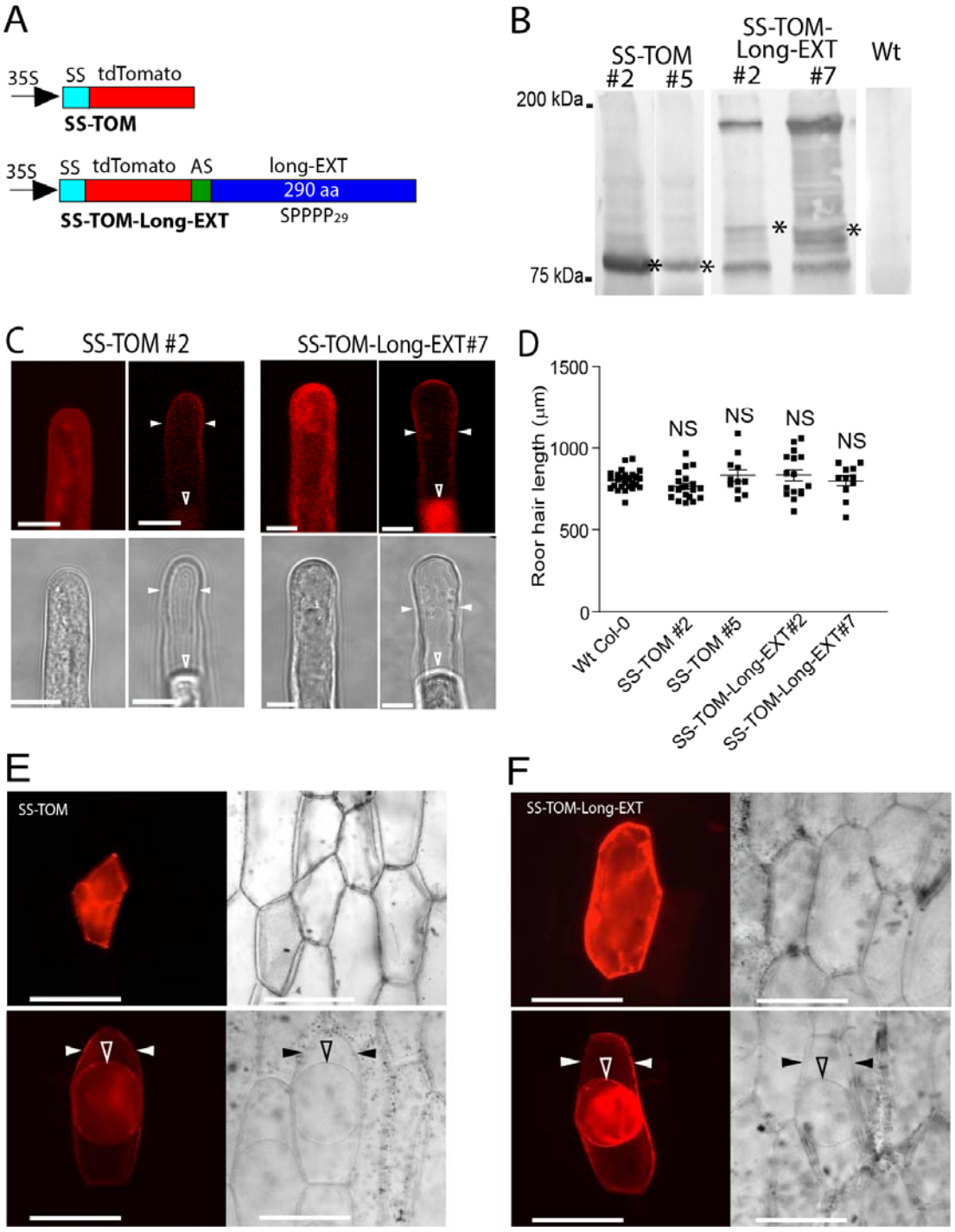

Figure S2. EXT reporter is targeted to root hair and onion epidermal cell walls.

(**A**) Schematic diagrams of SS-TOM and SS-TOM-Long-EXT constructs expressed under the control of the 35S promoter in Arabidopsis plants. SS, tomato polygalacturonase signal sequence. AS, Ala-spacer, 6 alanines between tdTomato (TOM) and Long-EXT domain. Long-EXT, C-terminal 290 amino acids of *SlPEX1*, which includes only two tyrosines at the C-terminus.

(**B**) Expression and detection of EXT-reporters in homozygous *Arabidopsis* lines. Lines expressing detectable levels of SS-TOM (lines #2 and #5) and SS-TOM-Long-EXT (lines #2 and #7) showed similarly unexpectedly large sizes of protein on the Western blot, with bands much larger than 94 kDa (the predicted size of the unmodified EXT protein). All the gel blots shown are part of the same run.

(**C**) Expression of SS-TOM and SS-TOM-Long-EXT reporters in *Arabidopsis* root hair cells. (Top) Fluorescence images showing cell-wall localization of the reporter protein: left, cells with normal cytoplasm; right, cells after plasmolysis in 1 M NaCl. (Bottom) Bright-field images of the same cells shown above. Cell wall location is denoted with solid arrowheads while plasma membrane is indicated with an unfilled arrowhead. Scale bar = 10 µm.

(**D**) Root hair phenotype of Wt, SS-TOM (#2 and #5) and SS-TOM-Long-EXT (#2 and #7) (in Wt background) as box-plot. Horizontal lines show the means. NS = not significantly different, determined by one-way ANOVA.

(**E**) Onion epidermis expressing SS-TOM. (On the right) Bright field images. (On the bottom) cells were plasmolyzed in 1 M NaCl. Cell wall location is denoted with solid arrowheads while plasma membrane is indicated with an unfilled arrowhead. Scale bar = 100 µm. SS = Signal Peptide. TOM = Tomato fluorescent protein.

(**F**) Onion epidermis expressing SS-TOM-Long-EXT. (On the right) Bright fields images. (On the bottom) Cells were plasmolyzed in 1 M NaCl. Cell wall location is denoted with solid arrowheads while plasma membrane is indicated with an unfilled arrowhead. Scale bar = 100 µm. SS = Signal Peptide. TOM = Tomato fluorescent protein. Long-EXT = C-terminal 290 amino acids of *Solanum lycopersicum* (Sl) *SlPEX1*.

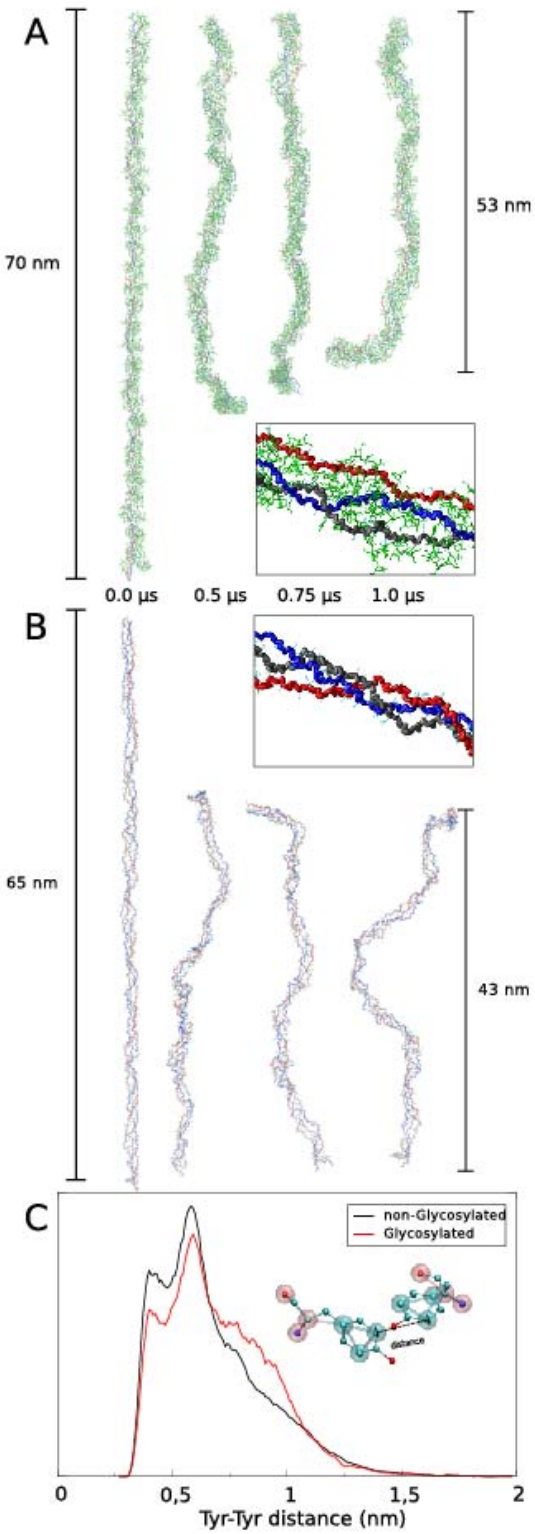

Figure S3. Effect of the *O*-glycosylation status on the triple helix EXT assembly and Tyr-Tyr distances.

Selected snapshots of the *O*-glycosylated (**A**) and non-glycosylated **(B)** triple EXT chain molecular dynamics (MD) trajectory, showing the stability of the triple helix during a 1 µs MD simulation. The results obtained in these simulations highlight the importance of the triple-helix EXT in overall protein stability, and especially the maintenance of the fibril-like structure. Peptide chains are depicted in red, black and blue and glycans in green. In these simulations the peptide chains are allowed to move freely inside the simulation box, without any restrictions. Insets: a snapshot of a 25 amino acid portion of the triple helix taken from the CG MD trajectory.

(**C**) Distribution of the Tyr-Tyr distances along the MD simulations for the glycosylated (red line) and non-glycosylated (black line) states. Distances are measured between the C-*ortho*s of each Tyr residue (as depicted in the inset of the figure).

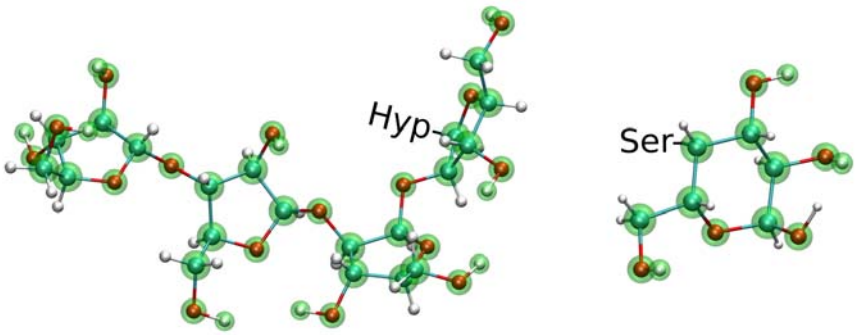

Figure S4. Coarse-grained models for tetra-arabinofuranose and galactopyranose moieties (diffuse green spheres) superimposed on all atom description (solid spheres connected by tubes). Interaction points or beads are located in the position of the heavy atoms and hydrogens corresponding to hydroxyl groups. The latter were included due to the importance of directional hydrogen bond-like interactions in this class of molecules. Mass and Lennard-Jones parameters of CG beads and spring constants for intramolecular interactions were chosen to be compatible with the SIRAH coarse-grained model (parameters are available upon request).

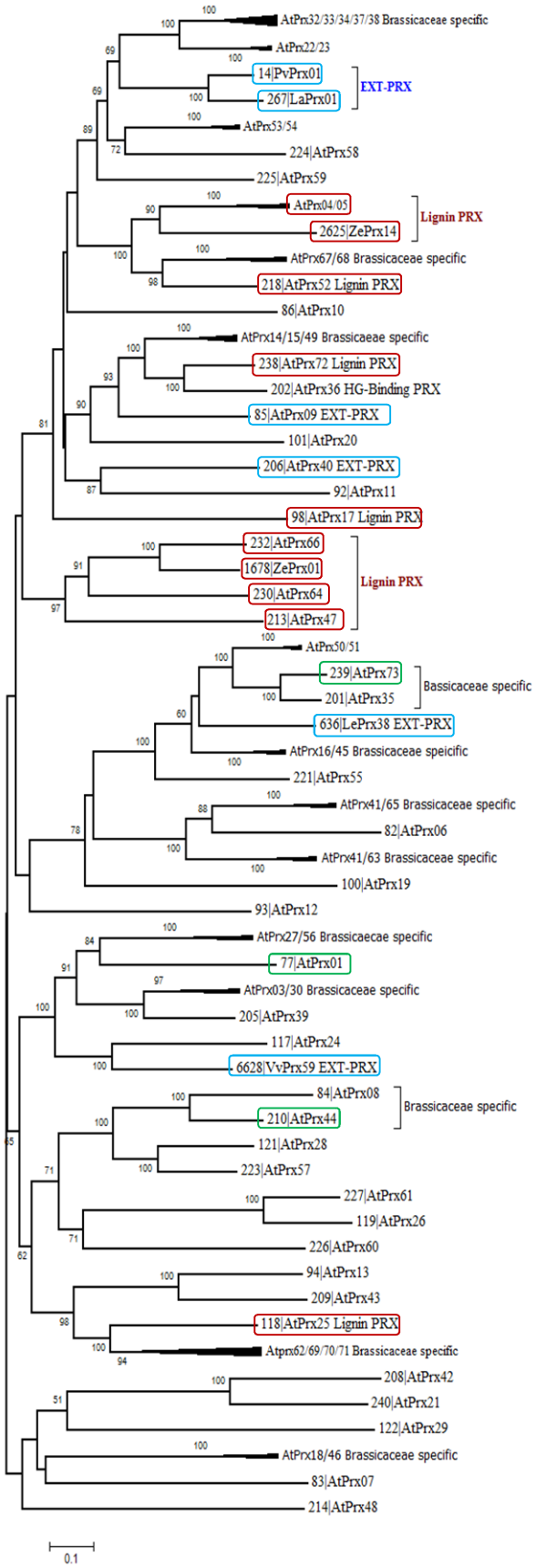

Figure S5. Evolutionary relationships of CIII Prx with putative extensin cross-linking activity.

The 73 Class III Peroxidase protein sequences from *A. thaliana,* two putative Lignin PRX from *Zinnia elegans* and four putative EXT-PRX from *Lupinus album, Solanum lycopersicum, Phaseolus vulgaris* and *Vitis vinifera*, have been aligned with ClustalW and the tree constructed using the Neighbor-Joining method (Saitou and Nei, 1987). The analyses were conducted in MEGA7 (Kumar, 2016). Class III PRXs with putative EXT-PRX activity or Lignin PRX activity were surrounded in blue and red respectively. The three Class III PRXs studied in the present work were surrounded in green. Branches of the tree with sequences resulting from duplication events only detected in Brassicaceae have collapsed to simplify the tree topology.

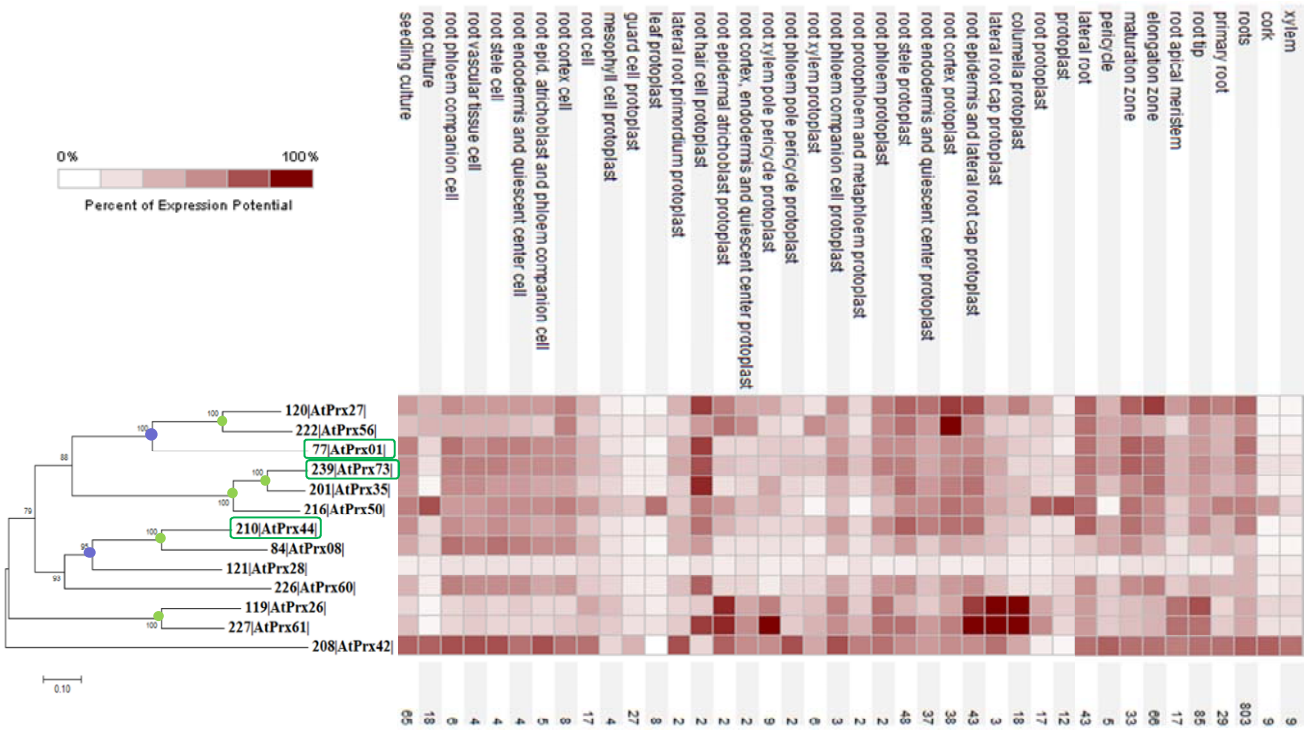

879

880 **Figure S6. Evolutionary and root tissue expression relationships of putative EXT-PRXs in**
881 **Arabidopsis.**

882 The evolutionary history of Class III PRXs in root hair associated has been conducted with 15 CIII PRX
883 protein sequences of *A. thaliana*. They have been aligned with ClustalW and the tree constructed
884 using the Neighbor-Joining method (Saitou and Nei, 1987). The analyses were conducted in MEGA7
885 (Kumar, 2016). The sequences of AtPRX01/02 and AtPRX50/51 are either identical or very close,
886 leading to only two independent expression profile from Affymetrix data. A brown (max value)-to-
887 cream (min value) heatmap was drawn from 105 anatomical parts from data selection available from
888 AT_AFFY_ATH1-0 and plotted in front of each branch and using Genevestigator. The 3 CIII PRX
889 studied in the present work were surrounded in green. Green and blue circles correspond to
890 duplication posterior to Brassicaceae and to Dicotyledons emergences respectively. All protein
891 sequences are available using their ID number (http://peroxibase.toulouse.inra.fr, (Savelli et al.,
892 2019). Numbers indicates the amount of dataset available for each tissue.

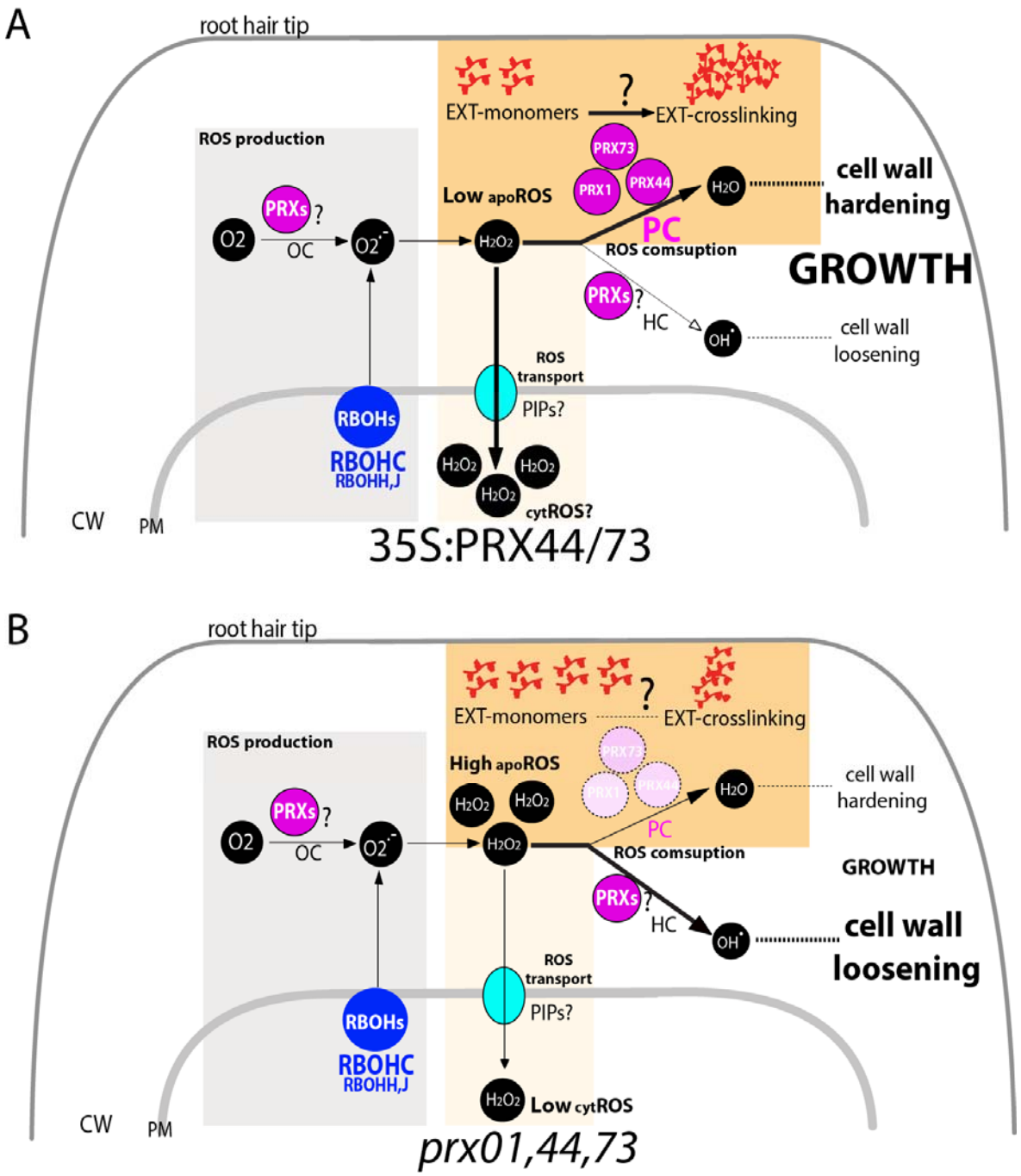

Figure S7. Current model of PRX01, PRX44, and PRX73 function linking ROS homeostasis and EXT crosslinking in the root hair cell walls. ROS homeostasis in the apoplast includes ROS production, ROS consumption, and ROS transport to the cytoplasm. ROS as superoxide ion ($O2^{-}$) is primarily produced by RBOHC and by RBOHH,J [based on Mangano et al. (2017)] and, possibly, by unknown PRXs in the root hair tip, and then dismutated to hydrogen peroxide (H_2O_2). (**A**) It is proposed that high levels of PRX44 or PRX73 during the peroxidative cycle (PC) (as found in 35S:PRX44-GFP and 35S:PRX73-GFP lines) might trigger a high consumption of apoplastic H_2O_2 (low $_{apo}$ROS) with a

902 concomitant cell wall hardening. (**B**) Under low levels of all three PRXs (as found in the triple mutant
903 *prx01,44,73*), most of the H_2O_2 produced accumulates in the apoplast (high $_{apo}$ROS) triggering a
904 cessation of cell expansion. A portion of apoplastic H_2O_2 might be transported into the cytoplasm by
905 aquaporins (PIPs). The balance between cell wall hardening and cell wall loosening processes might
906 be compromised, affecting polar root hair growth. CW = cell wall; PM = plasma membrane; HC =
907 hydroxylic cycle; OC = oxidative cycle. PIP= Plasma membrane Intrinsic Proteins (aquaporins).

SUPPLEMENTARY REFERENCES

Kumar, S., Stecher G., Tamura K. (2016) MEGA7: molecular evolutionaary genetic analysis version 7.0 for bigger datasets. *Mol. Biol. Evol.* 33(7): 1870-1874.

Mangano S. *et al.* (2017). The molecular link between auxin and ROS-controlled root hair growth. *Proc. Natl. Acad. Sci. U.S.A*. 114(20):5289-5294.

Marzol E, Borassi C, Bringas M, Sede A, Rodríguez Garcia DR, Capece L, Estevez JM. (2018). Filling the Gaps to Solve the Extensin Puzzle. *Mol Plant*. 11(5):645-658.

Mutwil, M., Klie, S., Tohge, T., Giorgi, F.M., Wilkins, O., Campbell, M.M., Fernie, A.R., Usadel, B., Nikoloski, Z. and Persson, S. (2011). PlaNet: combined sequence and expression comparisons across plant networks derived from seven species. *Plant Cell*, 23, 895– 910.

Saitou N, Nei M. (1987). The neighbor-joining method: a newmethod for reconstruction of phylogenetic trees. Mol Biol Evol4:406–25.

Savelli B., Li Q., Webber M., Jemmat A.M., Robitaille A., Zamocky M., Mathe C., Dunand C. (2019). RedoxiBase a database for ROS homeostasis regulated proteins. *Redox Biol*. doi.org/10.1016/j.redox.2019.101247.